Transport Properties of Quantum Point Contacts in The Presence of Edge States: Non-equilibrium vs. Equilibrated

G. Erbil Can Artun



YEDITEPE UNIVERSITY

Istanbul 2011

Yeditepe University
Department of Physics

Bachelor's Thesis

Transport Properties of Quantum Point Contacts in The Presence of Edge States: Non-equilibrium vs. Equilibrated

G. Erbil Can Artun

Supervisor: Prof. Avadis S. Hacınlıyan[1]
Co-supervisor: Assoc. Prof. Afif Sıddıki[2]

[1]*Physics Department, Yeditepe University, 34755, Istanbul, Turkey*
[2]*Physics Department, Istanbul University, 34452, Istanbul, Turkey*

Istanbul, Turkey
May 2011

Abstract

In this work, we investigated the electronic properties of two dimensional electron gas (2DEG) constrained by quantum point contacts (QPCs). We numerically studied the equilibration processes in the presence of a magnetic field by solving the three dimensional Poisson's equation self-consistently. We found a strong geometrical and likewise system parameter dependency on transport properties. Most interestingly, only by varying the magnetic field, one can manipulate the quantum device from non-equilibrium transport to equilibrium transport.

Özet

Bu çalışmada, kuantum nokta kontaklarla (KNK) zorlanan iki boyutlu elektron gazının (2BEG) elektronik özellikleri incelenmiştir. Üç boyutlu Poisson denkleminin öz uyumlu nümerik çözümü ile bir manyetik alan varlığında dengelenme süreci çalışılmıştır. Elektronik taşınma özellikleri üzerinde geometrik özelliklere ve sistem parametrelerine güçlü bir bağımlılık bulunmuştur. En ilginç olarak, sadece manyetik alan değiştirilerek, kuantum aygıtının dengesiz taşınımdan denge durumundaki taşınıma yönlendirebileceğimizi gözlemledik.

Contents

Acknowledgements

Abstract

Özet

1 Theoretical and Experimental Background 1

1.1 Introduction……...…1

1.2 Poisson's Equation…….2

1.3 Partial Differential Equations……...….3

1.4 Boundary Conditions…….4

1.4.1 Dirichlet Boundary Conditions…….....5

1.4.2 Neumann Boundary Conditions……...……5

1.5 Numerical Solution Methods for Differential Equations……...6

1.5.1 Euler Methods……...6

1.5.2 Runge-Kutta Methods…….10

1.5.3 Numerov Methods……...……...12

1.6 Est3D…….....…….……..13

1.6.1 Configuration of the Program…….....…….……..13

1.6.2 Output of the Program……...…….……..…16

1.6.3 Explanation of The Est3D Input File.....…….....…...…16

1.7 A Specific Example: Quantum Point Contact (QPC)……..17

1.7.1 Gate Defined Quantum Point Contact.....19

2 Theoretical Background on Magnetism 27

2.1 Hall Effect……..……...…...…….……27

2.2 Quantum Hall Effect……...……...…..……30

2.3 Edge States……...…...…….……...32

2.4 Local Ohm's Law……...…...…..…….34

3 Equilibration 36

3.1 Equilibrium……..36

3.2 Non-Equilibrium……...…39

3.3 Equilibration…….……40

4 Conclusion 42

Appendices 43

A Data Files 43

A.1 Input File For Est3D……..43

List of Figures 45

References 46

Chapter 1

Theoretical and Experimental Background

1.1 Introduction

In our new era, the use of knowledge and technology is at a very high level and it increases dramatically with time. By the increasing need of use of knowledge and technology, the interest on the quantum information processing has been increased a lot. This leads scientists and the engineers to investigate the electronic properties of the small-scale electronic devices. One of the most interesting and well studied of such devices is the so called quantum point contacts (QPCs). Aside from studying fundamentals of charge transport in mesoscopic conductors, QPCs can be used as very sensitive charge detectors. In view of quantum computation in solid-state systems, QPCs can be used as readout devices for the state of a qubit. A qubit or a quantum bit is a unit of quantum information in quantum computing. A QPC is simply a narrow constriction between two electrically conducting regions. QPCs are constructed on two dimensional electron systems (2DES). Via our current technology, we usually construct 2DES at the interface of an heterostructure. QPCs can be constructed either by inducing electrostatic potential on the plane of 2DES by depositing gates on the surface of the crystal and/or by chemically etching the structure. The small size of the constraint, that is in a scale such that quantum mechanical effects can be observed, creates quantized energy levels in one dimension (perpendicular to the current direction). Therefore, the charge transport takes place depending on whether the energy of the electron coincides with this quantized energy levels or not. Ideally, at low bias voltages, if the energy of the electron less than the lowest energy level of the constraint, no current can pass through the QPC. Otherwise, only a certain integer number of levels are involved, so the current is quantized. Some of the details of the QPC will be given in this report.

We said that QPCs can be used as very sensitive charge detectors. Since the conductance through the QPC strongly depends on the size of the constriction, any potential fluctuation in the vicinity will effect the current through the contact. Single electrons can be detected with such a scheme. However, aside from the physical size of the QPC, the perpendicular component of the applied magnetic field, B, is another parameter which induces quantization on the 2DES. The interesting physics dictated by this quantization is observed as the quantum Hall effect. Due to the perpendicular magnetic field, the energy spectrum of the system is discrete, like that of a harmonic oscillator. These energy levels are known as the Landau levels (LLs) and are given by $E_n = \hbar\omega_c(n+1/2)$, where n is a positive integer and cyclotron energy is defined as $\hbar\omega_c = \hbar eB/m$, where m is the effective mass of the electron. In the case

of electrostatic equilibrium, that is when a fixed electron density is satisfied, the Fermi energy, *Ef* , can either be pinned to one of the LLs, where the system is compressible or can fall in between two successive LLs. In the second case, there is no equilibrium, since there are no available states at the *Ef* for electrons to be redistributed so that the equilibrium can be satisfied again, the system is known to be incompressible. Within these incompressible regions the resistivity vanishes due to absence of scattering, hence all the applied current is confined to these regions.

We studied the transport in 2DES and to be able to control the current (in the future so that to use quantum information proccessing), we use the QPC and magnetic field. We tried to figure out the equilibration conditions.

In this work, we first give the theoretical and experimental background and then proceed with equilibration. In chapter 1, the experimental and theoretical background on electrostatic are given. First, in Sec. 1.1, Poisson's equation that is to be used to get the potential and electron distribution profiles of the 2DES, is given. Then the partial differential equations and their boundary conditions are given. In Sec. 1.5, some numerical methods to solve differential equations are given to understand the working mechanism of the programs that make computation numerically. In Sec. 1.6, the program we used that solves the Poisson's equation self-consistently is given. In the last section of chapter 1, a general introduction to QPCs is provided and the type that we used (gate defined QPC) is investigated as an example with the heterostructure we used and also the results from the Est3D calculations are analyzed. Theoretical background on magnetism is given in chapter 2. In chapter 3, equilibrium, non-equilibrium and equilibration cases are given respectively, and the results that we obtained are introduced. The final conclusion section includes a discussion of the findings.

1.2 Poisson's Equation

In solving electrostatic problems, we have a fundamental differential equation that must be satisfied by the potential $V(\vec{r})$ for given boundary condition(s), which will be discussed in this part.

We start by the elementary definition of the Gauss law, using the differential form,

$$\vec{\nabla} \cdot \vec{E} = \frac{\rho}{\varepsilon_0}, \tag{1.2.1}$$

where the operator $\vec{\nabla}(\vec{r})$ acts on the position dependent electric field $\vec{E}(\vec{r})$. We will use $\vec{E}$ and V instead of $\vec{E}(\vec{r})$ and $V(\vec{r})$ respectively, for convenience in the remaining. Hence, the electric field can be written as the gradient of a scalar potential,

$$\vec{E} = -\vec{\nabla} V . \tag{1.2.2}$$

Combining Eqs.(1.2.1) and (1.2.2), one obtains,

$$\vec{\nabla}\cdot(\vec{\nabla}V) = -\frac{\rho}{\varepsilon_0},$$

$$\nabla^2 V = -\frac{\rho}{\varepsilon_0}. \qquad (1.2.3)$$

This is known as the Poisson's equation. In the absence of any external charge density, the Poisson's equation reduces to a simpler form,

$$\nabla^2 V = 0, \qquad (1.2.4)$$

which is known as Laplace's equation.

The operator ∇^2 involves differentiation with respect to more than one variable. Hence, Poisson's equation is a partial differential equation that may be solved once it is known that the functional dependence of $\rho(x,y,z)$ and the appropriate boundary conditions. [1]

1.3 Partial Differential Equations

There are two or more independent variables in many real physical problems, so the corresponding mathematical models involve partial differential equations rather than ordinary ones. Partial differential equations are solved generally by separation of variables and the replacement of the partial differential equations by a set of ordinary differential equations that must be solved subject to a given initial or boundary conditions. The solution of the partial differential equation is then expressed as a sum of the solutions coming from the ordinary differential equations, and they are usually infinite series; as Fourier series. [2]

Physical applications often lead to such problems that the value of the dependent variable y, or its derivative is specified at two different points; boundary conditions. A differential equation with boundary conditions form a two-point boundary value problem. For example let's consider a typical differential equation,

$$y''+p(x)y'+q(x)y = g(x), \qquad (1.3.1)$$

with the boundary conditions,

$$y(c_1) = y_0, \quad y(c_2) = y_1. \qquad (1.3.2)$$

To be able to solve the boundary value problem (1.3.1), (1.3.2) it is needed to find a function $y = \varphi(x)$ that satisfies the diferential equation (1.3.1) in the interval $c_1 < x < c_2$ and that takes the boundary values (1.3.2) at the end points of the interval. It is common to find a general

solution to the differential equation first, then the boundary conditions are imposed to determine the values of the arbitrary constants.

One of the most important partial differential equation is the Laplace's equation. Since, our aim is to model electronic transport in two-dimensions we consider,

$$\frac{\partial^2 u}{\partial x^2} + \frac{\partial^2 u}{\partial y^2} = 0 . \qquad (1.3.3)$$

To uniquely determine the solution of a given differential equation one has to fix the time and spatial boundary conditions. If there is no time dependence in the problem, as for Laplace's or Poisson's equations, there are no initial conditions to be satisfied. As in all differential equations, the Laplace equation should also satisfy certain boundary conditions on the boundary of a curve or a surface of the region in which the differential equation is wanted to be solved. The problem of finding a solution of the Laplace's equation that considers only the boundary values is known as Dirichlet problem, whereas, if the values of the normal derivative are prescribed on the boundary, the problem is known as the Neumann problem. The conditions of these problems are called Dirichlet boundary conditions and Neumann boundary conditions, respectively, and they are illustrated in the following section.

1.4 Boundary Conditions

There are three types of boundary conditions commonly encountered in the solutions of partial differential equations [3]:

Dirichlet boundary conditions: The value of a function is specified on the boundary. By the function, it is meant that the potantial, in electrostatics.

Neumann boundary conditions: The normal derivative of a function is specified on the boundary. In electrostatics, this would be the normal component of the electric field or alternatively the surface charge density.

Cauchy (mixed) boundary conditions: It means Dirichlet plus Neumann boundary conditions. The value of a function and its normal derivative are specified at the boundary. In electrostatics, this means the potential and the normal component of the electric field.

For example, for Poisson's equation with a closed surface, both Dirichlet and Neumann boundary conditions can lead to a unique, stable solution. Therefore, Cauchy boundary conditions can lead to an inconsistency, which one should be aware of and investigate carefully the properties of the physical system. [2]

We will be discussing in more detail the Dirichlet and the Neumann boundary conditions in the following parts.

1.4.1 Dirichlet Boundary Conditions

The Dirichlet boundary condition was named after Johann P. G. L. Dirichlet. For an ordinary or a partial differential equation, the Dirichlet boundary conditions specify the values that the solution has to satisfy on the boundary of the domain.

For an ordinary differential equation such as:

$$\frac{d^2y}{dx^2} + ay = b,$$

on the interval $[c_1, c_2]$, the Dirichlet boundary conditions take the form:

$$y(c_1) = \alpha_1,$$
$$y(c_2) = \alpha_2,$$

where α_1 and α_2 are given (real) numbers. For a partial differential equation on a domain Ω such as:

$$\nabla^2 y + y = 0,$$

the Dirichlet boundary condition takes the form:

$$y(x) = f(x),$$

where f is a known function defined on the boundary $\partial\Omega$.

1.4.2 Neumann Boundary Conditions

The Neumann boundary condition was named after Carl von Neumann. For an ordinary or a partial differential equation, the Neumann boundary condition specifies the values that the derivative of a solution is to take on the boundary of the domain.

For an ordinary differential equation such as:

$$\frac{d^2y}{dx^2} + ay = b$$

on the interval $[c_1, c_2]$, the Neumann boundary conditions take the form:

$$\frac{dy}{dx}(c_1) = \alpha_1,$$

$$\frac{dy}{dx}(c_2) = \alpha_2 ,$$

where α_1 and α_2 are given numbers.

For a partial differential equation on a domain Ω such as:

$$\nabla^2 y = 0 ,$$

the Neumann boundary condition takes the form:

$$\frac{\partial y}{\partial n}(x) = f(x) ,$$

where n denotes the normal to the boundary $\partial\Omega$ and f are given scalar functions. The normal derivative which is on the left-hand side is defined as:

$$\frac{\partial y}{\partial n}(x) = \vec{\nabla} y(x) \cdot \hat{n}(x) .$$

1.5 Numerical Solution Methods for Differential Equations

Numerical solutions of differential equations are quite important in computational physics, because it can be said that the study of physics is the study of differential equations, to a large extent. In real life, there are nearly no “linear second-order homogeneous differential equations with constant coefficients”. However, all the interesting equations are either trivial or impossibly difficult to solve analytically. These “difficulties” can be handled by numerical methods. In this chapter, we used references [4, 5, 6, 7, 8], and the lecture notes of Prof. A. Hacınlıyan.

Unforunately, there is no way to determine the best method for solving all equations. Each equation has a special character. One method can work well for one differential equation while it does not for another. In this part, some methods that are shown to be useful to solve a differential equation will be given.

1.5.1 Euler Methods

Let’s consider the equation,

$$y'(x) = f(x, y) . \qquad (1.5.1)$$

It should be noted that if f is a function of x alone, it can be solved immediately for y as following,

$$y(x) = \int^{x} f(x')dx' . \tag{1.5.2}$$

Since, this is an uninteresting situation, it will be assumed that f is a function of x and y. Eq.(1.5.1) can be solved by Taylor series. If all the derivatives are known, the solution can be constructed from the expansion,

$$y(x) = y(x_0) + (x - x_0)y'(x_0) + \frac{(x - x_0)^2}{2!} y''(x_0) + \ldots \tag{1.5.3}$$

since $y'(x)$ is known, higher derivatives can be obtained, but a little work is required. The second derivative is,

$$\begin{aligned} y''(x) &= \frac{\partial}{\partial x} f(x,y) + \frac{dy}{dx}\frac{\partial}{\partial y} f(x,y) \\ &= \frac{\partial}{\partial x} f(x,y) + f(x,y)\frac{\partial}{\partial y} f(x,y) . \end{aligned} \tag{1.5.4}$$

Clearly this leads to some complicated expressions, and the situation degenerates as it is moved to higher derivatives. As a practical matter, the Taylor series solution is not very helpful. However, it provides criteria that other methods can be measured. To that end, it is written as,

$$\begin{aligned} y(x) = y_0 + (x - x_0) f(x_0, y_0) + \frac{(x - x_0)^2}{2!}\left[\frac{\partial f(x_0, y_0)}{\partial x} + f(x_0, y_0)\frac{\partial f(x_0, y_0)}{\partial y}\right] \\ + \frac{(x - x_0)^3}{3!} y'''(\xi), \end{aligned} \tag{1.5.5}$$

where $y_0 = y(x_0)$.

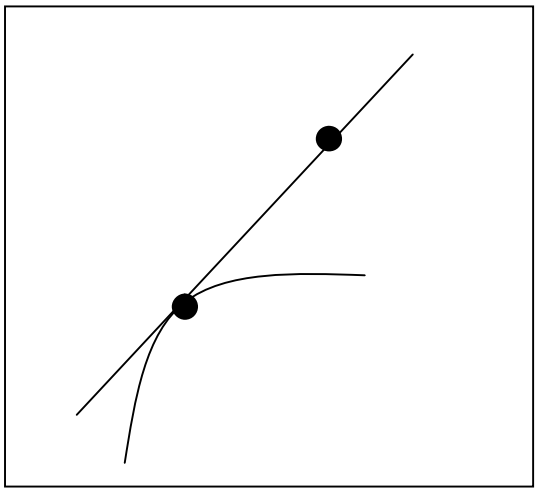

Figure 1.5.1: The simple Euler method.

The original differential equation gives the derivative y' at any point; if it is given that the value of y at some point x_0, then the function can be approximated by a Taylor series, including only first two terms,

$$y(x) \approx y(x_0) + (x - x_0)y'(x_0) . \qquad (1.5.6)$$

This method seems to be easy, but it actually works. However, the accuracy of the solution is doubtful. Denoting the size of the step $(x - x_0)$ by h, Eq.(1.5.6) can be written as an equality,

$$y(x_0 + h) = y(x_0) + hf(x_0, y(x_0)) = y_0 + hf_0 , \qquad (1.5.7)$$

where, $y_0 = y(x_0)$ and $f_0 = f(x_0, y_0)$. This is know as the (simple) Euler method, and it allows to move the solution along, one step at a time, as indicated in Figure 1.5.1. A typical implementation is to derive the total integration region into steps of size h, and to move the solution along one step at a time in an obvious way. To check the accuracy, the calculation can be repeated for a different step sizes and the results can be compared.

There is a problem with the simple Euler method; the derivative at the beginning of the interval is assumed to be constant over the entire step. Note that, such asymmetric treatments always lead to low accuracy in the solution. Using a median value of the derivative, for instance a halfway through the step, would yield a solution with a higher accuracy. The question now is how to evaluate the derivative at the midpoint, when the derivative is itself a function of y?

Let's use the Euler's method to guess the solution at the midpoint, $x_{mid} = x_0 + h/2$. Namely,

$$y(x_{mid}) = y_0 + \frac{h}{2}y'_0 = y_0 + \frac{h}{2}f_0 , \qquad (1.5.8)$$

where it's been again associated the derivative of y with the funciton f. Utilizing this expression for $y(x_{mid})$, one can evaluate the derivative at the midpoint, $f(x_{mid}, y_{mid})$. In addition, approximating the derivative over the entire interval one obtains,

$$y(x_{mid}) = y_0 + \frac{h}{2} y'_0 = y_0 + \frac{h}{2} f_0 . \qquad (1.5.9)$$

This is the modified Euler's method, and it has an interesting geometrical interpretation. (See Figure 1.5.2). While Euler's method corresponds to drawing a straight line through (x_o,y_o), but with (approximately) the derivative at the midpoint of the interval. In other words, this method considers a simple approximation to the derivative at the midpoint,

$$f(x_{mid}, y_{mid}) = y'(x_{mid}) \approx \frac{y(x_0 + h) - y(x_0)}{h} . \qquad (1.5.10)$$

Using Euler's method for an approximate y_{mid}, the modified Euler method quickly follows.

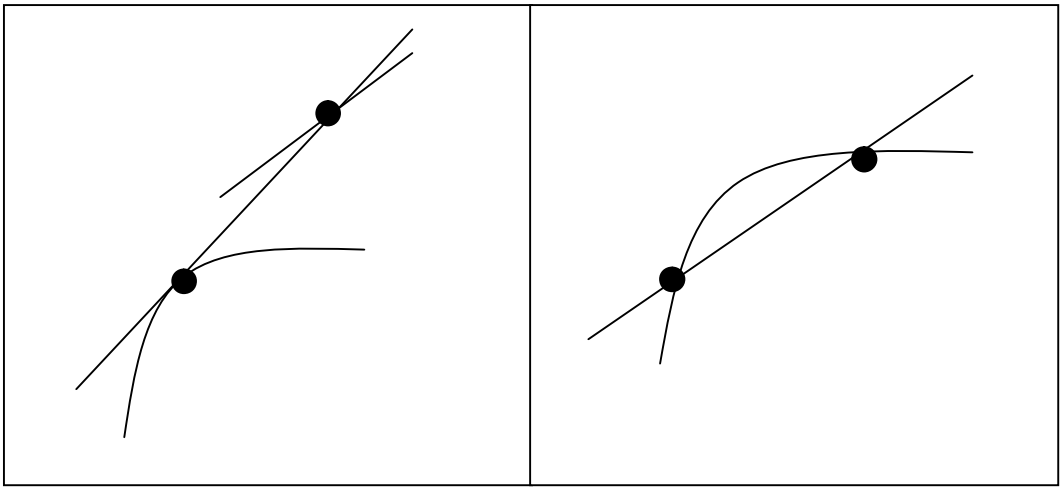

Figure 1.5.2: The modified Euler method.

Yet another variation of Euler's method is possible if solution is attempted using a mean value of the derivative. (See Figure 1.5.3). That is, the Euler's equation is used to guess at $y(x_0 + h)$, and is utilized to evaluate the derivative at the end of the interval. This derivative is averaged with the "known" derivative at the begining of the interval, and this mean derivative is used to advance the solution. The improved Euler method is thus given as,

$$y(x_0 + h) = y(x_0) + \frac{f_0 + f(x_0 + h, y_0 + h f_0)}{2} . \qquad (1.5.11)$$

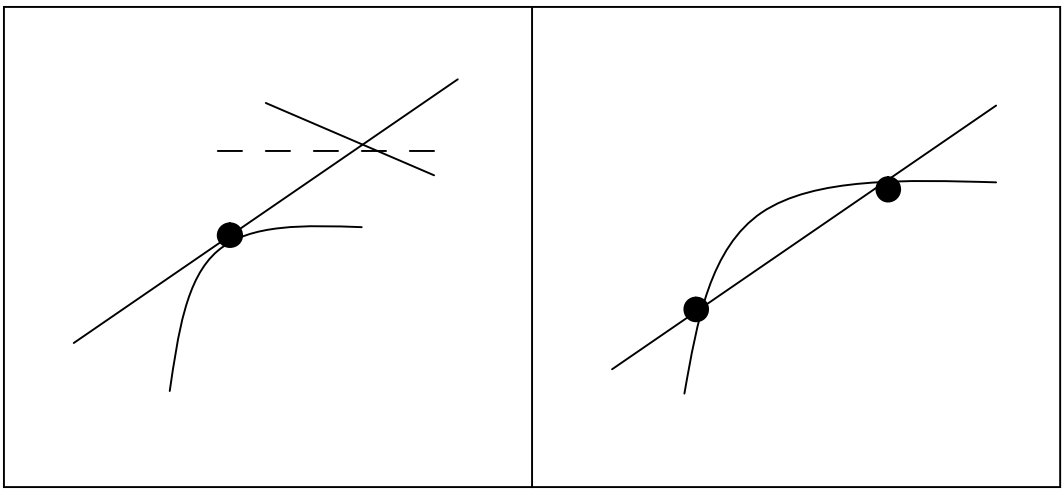

Figure 1.5.3: The improved Euler method.

1.5.2 Runge-Kutta Methods

There is a large freedom in writing down algorithms for integrating differential equations and each has its own peculiarities and advantages. Runge-Kutta algorithms are widely used, which present varying orders of accuracy. A second-order version is derived here to give the spirit of the approach and then the equations for the third- and commonly used fourth-order methods can be simply stated. To derive a second-order Runge-Kutta algorithm, f in the integral of,

$$y_{n+1} = y_n + \int_{x_n}^{x_{n+1}} f(x,y)dx, \qquad (1.5.12)$$

is approximated by its Taylor series expansion about the mid-point of the interval. Thus,

$$y_{n+1} = y_n + hf(x_{n+1/2}, y_{n+1/2}) + O(h^3), \qquad (1.5.13)$$

where the error aries from the quadratic term in the Taylor series, as the linear term integrates to zero. Although, the equation seems to impose that the value of $y_{n+1/2}$ in the right hand side should be known, this is not true. Since the error term is already of the order of $O(h^3)$, an approximation to y_{n+1} whose error is $O(h^2)$ is already sufficient. This is provided by the simple Euler's method, $y_{n+1} = y_n + hf(x_n, y_n) + O(h^2)$. Thus, if k is defined to be an intermediate approximation to twice the difference between $y_{n+1/2}$ and y_n, the following two-step procedure gives y_{n+1} in terms of y_n,

$$k = hf(x_n, y_n); \qquad (1.5.14.a)$$

$$y_{n+1} = y_n + hf(x_n + h/2, y_n + k/2) + O(h^3). \qquad (1.5.14.b)$$

This is the second-order Runge-Kutta algorithm. It embodies the general idea of substituting approximations for the values of y into the right-hand side of implicit expessions involving f. It is as accurate as Taylor series or implicit methods, but places no special constraints on f, such as easy differentiability or linearity in y. It also uses the value of y at only one previous point, in contrast to the multipoint methods discussed above. However, Eq.(1.5.14) requires the evaluation of f twice for each step along the lattice. Runge-Kutta schemes of higher-order can be derived in a relatively straightforward way. Any quadrature formula can be used to approximate the integral (1.5.12) by a finite sum of f values. For example, Simpson's rule yields, (notation change $f(x+h/2) \to f_{n+1/2}$)

$$y_{n+1} = y_n + \frac{h}{6}\left[f(x_n, y_n) + 4f(x_{n+1/2}, y_{n+1/2}) + f(x_{n+1}, y_{n+1})\right] + O(h^5). \qquad (1.5.15)$$

Schemes for generating succesive approximations to the y's appearing in the right-hand side of a commensurate accuracy completes the algorithms. A third-order algorithm with a local error $O(h^4)$ is,

$$\begin{aligned} k_1 &= hf(x_n, y_n); \\ k_2 &= hf(x_n + h/2, y_n + k_1/2); \\ k_3 &= hf(x_n + h, y_n - k_1 + 2k_2); \\ y_{n+1} &= y_n + \frac{1}{6}(k_1 + 4k_2 + k_3) + O(h^4). \end{aligned} \qquad (1.5.16)$$

It is based on Eq.(1.5.15) and requires three evaluations of f per step. A fourth-order algorithm, which requires f to be evaluated four times for each integration step and has a local accuracy of $O(h^5)$, has been found by experience to give the best balance between accuracy and computational effort. It can be written as follows, with the k_i as intermediate variables,

$$\begin{aligned} k_1 &= hf(x_n, y_n); \\ k_2 &= hf(x_n + h/2, y_n + k_1/2); \\ k_3 &= hf(x_n + h/2, y_n + k_2/2); \\ k_4 &= hf(x_n + h, y_n + k_3); \\ y_{n+1} &= y_n + \frac{1}{6}(k_1 + 2k_2 + 2k_3 + k_4) + O(h^5). \end{aligned} \qquad (1.5.17)$$

1.5.3 Numerov Method

There is a particular simple and efficient method for integrating second-order differential equations having the form of,

$$\frac{d^2y}{dx^2} = k^2(x)y = S(x). \tag{1.5.18}$$

To derive this method, commonly called the Numerov or Cowling's method, it is begun by approximating the second derivative in Eq.(1.5.18) by the three-point difference formula*,

$$\frac{y_{n+1} - 2y_n + y_{n-1}}{h^2} = y_n'' + \frac{h^2}{12} y_n'''' + O(h^4), \tag{1.5.19}$$

where it has been written out explicitly that the $O(h^2)$ "error" term, which is derived easily from the Taylor expansion. From the differential equation itself, it is had,

$$\begin{aligned} y_n'''' &= \frac{d^2}{dx^2}(-k^2y + S)\Big|_{x=x} \\ &= -\frac{(k^2y)_{n+1} - 2(k^2y)_n + (k^2y)_{n-1}}{h^2} \\ &\quad + \frac{S_{n+1} - 2S_n + S_{n-1}}{h^2} + O(h^2). \end{aligned} \tag{1.5.20}$$

When this is substituted into Eq.(1.4.19), it can be written, after some rearrangement that,

$$\begin{aligned} &(1 + \frac{h^2}{12}k_{n+1}^2)y_{n+1} - 2(1 - \frac{5h^2}{12}k_n^2)y_n + (1 + \frac{h^2}{12}k_{n-1}^2)y_{n-1} = \\ &\quad \frac{h^2}{12}(S_{n+1} + 10S_n + S_{n-1}) + O(h^6). \end{aligned} \tag{1.5.21}$$

Solving this linear equation for either y_{n+1} or y_{n-1} then provides a recursion relation for integrating either forward or backward in x, with a local error $O(h^6)$. It should be noted that this is one order higher in accuracy according to the fourth-order Runge-Kutta method Eq.(1.5.17), which might be used to integrate the problem as two coupled first-order equations. The Numerov scheme is also more efficient, as each step requires the computation of k^2 and S at only the lattice points.

---

* The three-point difference formula is given as, $\frac{\partial^2 f}{\partial x^2} = \frac{f(x+h) - 2f(x) + f(x-h)}{h^2} + O(h^2)$.

1.6 Est3D

Est3D (Electrostatics in three dimension) software package was written by Anderas Weichselbaum, Arnold Sommerfeld Center/Ludwig Maximilians Universitat, and further adapted and modified by Sefa Arslan for the structures that we are interested in. As a development environment, C++ programming language is used. References [9] and [10] were utilized for this section.

To obtain electrostatic potential landscapes, the solution of the Laplace's or Poisson's equation is needed and it is a well defined boundary value problem, requiring the discretization of space on a convenient grid. Relaxation techniques are usually used for these problems. Relaxation techniques provide efficient algorithms such as multi-grid, Jacobi, and Gauss-Seidel iteration schemes.

The three-dimensional numerical algorithm used in this program is adapted from the well-known numerical relaxation technique for solution of the Poisson equation in 2D. Using the self-consistent iteration scheme all the charges in the system are calculated accurately to satisfy the desired boundary conditions. The program solves the Poisson's equation self-consistently with open boundary conditions by considering up to fourth order degree neighbour effects and gives the electron density and potential distributions. In three dimensions, however, due to the poor scaling with grid dimensions, better algorithms are desirable.

1.6.1 Configuration of Application

In this section, configuration parameters of the Est3D application will be discussed. The program parameters are kept in two ways, via the environmental variables and the computation data file. Preparation of the data file will be discussed in Sec. 1.6.3, but here a general introduction will be given.

Input File

The sample which will be simulated has to be defined in **est3.dat** data file. The measurable quantities like the physical size of the system, computational grid size, amount of the charges, location of the gates and the voltage that are imposed on the boundaries, impurities and properties of the dielectric material should be defined at the input file.

The variable **SYS_PARAS** in the data file defines the dimensions of the system. The format of the parameter is like following:

SYS_PARAS = [NX NY NZ LX fhY fhZ]

NX, NY and NZ stands for the dimensions of the computational grid in x-, y- and z-directions respectively. LX is the physical dimension of the system in x-direction. The grid spacing h_x is calculated by $LX/(NX-1)$ at x, fhY and fhZ adjust the grid size such that and h_y and h_z are calculated by $h_y = (\text{fhY}.\ h_x)$ and $h_z = (\text{fhZ}.\ h_x)$ respectively.

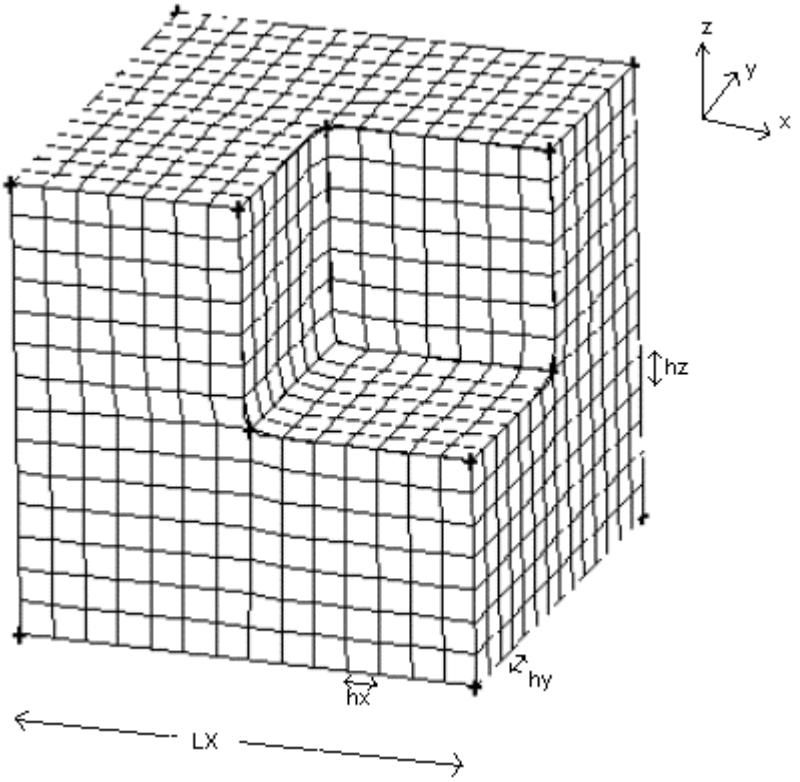

Figure 1.6.1: Schematic representation of the structure defined by the program in grid dimensions.

Non-geometric surfaces, etching or gating patterns which are defined via the individual coordinates of each grid points on the pattern profile has to be defined in a ***.srf** file, like gates.srf. The pattern file and the patterns included by the file should be set in the data file via **BDR_FILE** variable, that fixes the boundary conditions. The format of the variable is as follows:

```
BDR_FILE = {
pattern_file    SX  SY  SZ   bXY   bZ
pattern_name VX  VY  VZ  'type'  'value'
}
```

Here SX, SY, SZ represents the starting point for the shifting of coordinates, if necessary, and bXY, bZ represents the value of shifting. VX, VY and VZ indicates where the patterns will be placed, on which plane, xy xz or yz, and on which layer of the plane. The 'value' parameter is assigned to each grid point for the given pattern. It is possible to use as many patterns as

needed. The given pattern may be used for different purposes -etching, gating etc.- and can represents different type of structures. The list of 'type' identifiers is as following:

C : Point charge

C2 : 2D charge distribution

D : Dielectric boundary

E : Etched boundary

V : Boundary with given voltage.

VO- : Boundary with given negative voltage

ISLANDS variable defines the geometric structures. The format is as following:

ISLANDS = { 'structure name' I1 J1 K1 I2 J2 K2 'type' value }

Here I1, J1 and K1 indicate the starting points of the structure while I2, J2, and K2 are the end points in x-, y-, z-directions respectively. If the size of the structure is only 1 grid point in the given plane, it is enough to use "~" character for the end point coordinate. The same considerations are valid for the 'type' and 'value' parameters discussed above. It is possible to use many structures to simulate nearly real systems.

An example data file for a system that was used in our work (it will be looked in detail in the following section):

```
%SETUP DIMENSIONS

                %   NX0  NY0 NZ0  LX       fhY    fhZ
SYS_PARAS = [  128   128   137   2.0E-6   1.0   0.4762  ]

BDR_FILE  =  {
%     FILE NAME  -- SHIFT_X, Y, Z  -  bXY  -  bZ ----------------------------------
        'gates.srf'                  0   0   0      6        6     'file'  %  user structure

%    VARNAME – SHIFT_X, Y, Z - [VQ]  VALUE   -   DESCRIPTION --------
        'qpc'                    0   0   0    68      'V'    'disa gate'    % gate

ISLANDS = {
% VARNAME  ----   I1   J1   K1  --  I2    J2    K2  --  [VQ]  -  VALUE ------------
        'dielec'          3    3    3       124 124  92         'D'         12.0
        'surf'            6    6    91      121 121  ~          'VO-'       -0.75
```

```
        'donors1'    6   6   69   121 121  ~    'C2'    2.50E15
        'donors2'    6   6   86   121 121  ~    'C2'    1.70E16
        '2DEG'       6   6   53   121 121  ~    'VO-'   0.0
}
```

1.6.2 Output of the Program

When the execution of the program ends, it produces an output file which has the name **V00.mat.** All the information including the voltage and charge distributions on the grid points is effused as binary. The data has the Matlab format, so the output files can be anaylzed by matlab functions.

1.6.3 Explanation of The Est3D Input File

In this part, preparation of the input file of the quantum point contact, introduced at Figure 1.7.2, will be described step by step.

The system of interest consists of several components and it is defined in section 1.7.1.

The dielectric coefficient of AlGaAs and GaAs are approximately the same, $\varepsilon = 12.4\ \varepsilon_0$, therefore these two set of layers may be treated as they are a single thick layer with 660 nm of thickness. The thickness of upper and lower parts are 285 nm and 375 nm respectively. The two-dimensional electron system is formed at the interface of AlGaAs and GaAs. The 2DEG thickness will be assumed as one computational layer (dz), 7.5 nm. Two donor (δ) layers embedded into AlGaAs layer at 37.5 nm and 180 nm depth from the surface respectively. The

distance between the lower donor layer and the 2DEG layer is 120 nm. The length of the material in $x-$ and $y-$ directions are the same and equal to 1500 nm.

The real and the computational dimensions of the system should be provided by **SYS_PARAS** variable in the input file. For our sample simulation, the described construction will be transfered into 128x128x32 (x,y,z) computational grid. Longer execution time and larger physical memory are required to make computation with larger grid sizes with Est3D. The fields for grid sizes NX, NY, NZ are integer type entries. The physical lengths Lx and Lz are the real size of the construction in unit of meters.

The geometric structure, the layers and the properties of the layers (donors, 2DEG, dielectric layers), is defined by **ISLANDS** variable in the input file. As stated before, dielectric material is consisting of upper and lower parts and since the electrical properties of these parts are relatively similar, they may be treated as a single material with dielectric constant $\varepsilon = 12.0\ \varepsilon_0$. The total thickness of the component equals to 88 computational grids. Starting from the bottom, 0th layer, the component placed between 3rd and 91th layers. For computational reasons, a distance with three-layer thickness should be inserted between the dielectric and the

border. Due to the same reasons *x* and *y* dimensions of the component is defined between 3rd and 124th grid points at *xy* plane. The type identifier for dielectric is **D** as stated in page 14.

Approximately 10% of donated electrons by the ionized donors escapes to the surface and induce a homogeneous voltage distribution about 0.75 V (for the given amount of donors). To represent this situation in the simulation, a metallic surface layer is placed just one layer below the top layer of the dielectric grid. For the stability concerns of the simulation results, three grid points distance is kept between the dielectric material and the metallic surface at *xy* plane. Since the surface is metallic it can keep only electrons. The type identifier for this layer is **V0-**.

The donors are placed at the 69th. and 89th. layers. Donors are assumed to be homogeneously distributed over one computational unit thickness of layer. The donor layers can be treated as two dimensional charge distributions with the density of 2.5 x 10^{15} m^{-2} and 1.7 x 10^{16} m^{-2} respectively from lower donor layer to upper one. The type identifier for this layer is **C2** (page 14).

To use non-geometric patterns as a component, the coordinate information of each point in the pattern should be provided in a pattern input file. For a system which has 128x128 grid points at its *xy* plane, the number of the points to be proceeded is 16384. It is not possible to handle that amount of grid points by hand. So, we use a program that creates a data file for the pattern. It defines the etching or gating pattern via individual coordinates of each grid point on the pattern profile. The pattern profile is needed to be defined in a ***.srf** file and it is identified in the input file via **BDR_FILE** variable.

A full input file that is used in our work can be found in Appendix A.

1.7 A Specific Example: Quantum Point Contact (QPC)

A quantum point contact (QPC) is simply a very narrow (a width comparable to the electronic wavelength; nano- to micrometer) constriction between two electrically conducting regions in very small scale in which quantum mechanical effects can be observed. QPCs can be created on a two-dimensional electron gas (2DEG) via inducing narrow contsrictions by depositing gates on the surface of the crystal. QPCs were reported firstly by Van Wees et al. and Wharam et al. in 1988. References [9, 11, 12, 18] were utilized in this section.

A quantum point contact presents a resistance to the motion of electrons in transverse direction. The current that is flowing through the contact is given by $I = GV$, where V is the potantial that is applied accross the contact and G is the conductance of the contact. This formula is similar to the Ohm's law for macroscopic resistors and the conductance G here can be thought as the quantum mechanical version of the conductivity σ for macroscopic resistors. As can be guessed from the name of the QPCs, quantum mechanical behavior of the nature and of the electrons should be taken into account, because of the small sizes. QPCs creates a potential barrier perpendicular to the current direction and it quantizes the energy levels. That is, the electrons which are at only the certain energy states can pass through the energy barrier created by the QPC (see Figure 1.7.1) and only these electrons can contribute

to the current. Thus, at low temperatures and voltages, the electrons that contribute to the current can have only certain values of wavelength, energy and momentum which are also called the Fermi wavelength, energy and momentum respectively. Therefore, the electrons are considered to be plane waves before they reach to the QPC and quantum mechanical solutions are carried out and transmission and reflection coefficients are calculated. We have used the results of these calculations in our work.

a)

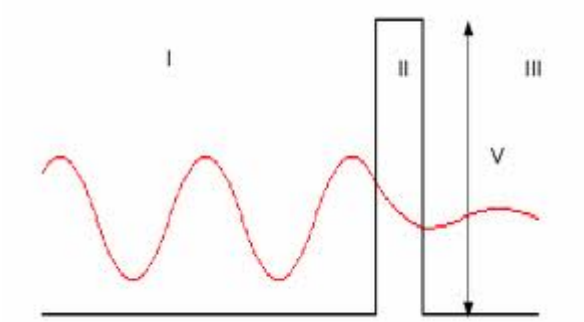

b)

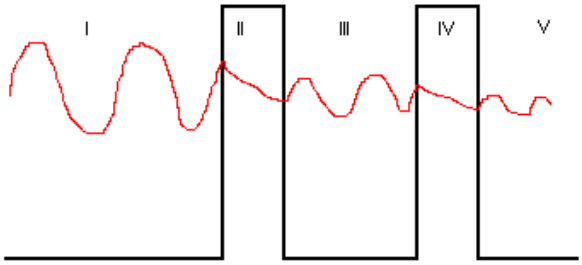

Figure 1.7.1: a) Tunneling through a potential barrier, say created by a QPC. The region I represents the region that the electron is in, before it reaches the QPC (the potential barrier), The region II shows the potential barrier created by the QPC. V is the potential energy of the barrier. **b)** Tunneling through two potential barriers, say created by double QPC. The region I represents the region that the electron is in, before it reaches the QPC, II and III are the barriers. III shows the region between the QPCs.

The electron wave can only pass through the constriction if it interferes constructively which for a given size of constriction only happens for a certain number of modes *N*. The induced current is given by the product of the electron velocity and the electron density. As a result, each state contributes the same amount e^2/h per spin direction to the total conductance,

$$G = NG_Q . \qquad (1.7.1)$$

G_Q is said to be the conductance quantum and it is given by,

$$G_Q = 2e^2 / h \ , \qquad (1.7.2)$$

where e is the elctron charge and h is the Planck's constant. The integer number N is determined by the width of the point. Thus, the total conductance is quantized and does not take on arbitrary values. As a function of the width (or gate voltage in the case of GaAs/AlGaAs heterostructure devices) of the QPC, the conductance shows a staircase behaviour (see Figure 2.2.2) as more and more modes (or channels) contribute to the electron transport. The step-height is given by Eq.(1.7.2).

For QPCs, the common starting point for the investigation of the structures is the degenerate two-dimensional electron gas (2DEG), present at the interface between GaAs and AlGaAs layers in a heterostructure (see Figure 1.7.2). The electrons are confined in the GaAs by a potential well at the interface with the AlGaAs, which results from the repulsive barrier due to the conduction band ofset between the two semiconductors, and from the attractive electrostatic potential due to the positively charged ionized donors in the AlGaAs layer. The electrons thus are confined in a direction normal to the interface, but they are free to move along the interface. This implies that a two-dimensional subband is associated with each discrete confinement level in the well. Usually, the potential well is quite narrow (about 10 nm) that only a single two-dimensional subband is occupied, and the density of states is strictly two-dimensional. At low temperatures, these states are occupied up to the Fermi energy, E_F. Additional confinement occurs in a lateral direction if a narrow channel is defined electrostatically in the 2DEG. This leads to the formation of one-dimensional subbands, characterized by free motion in a single direction.

1.7.1 Gate Defined Quantum Point Contact

Point contacts in metals act like small conducting orifices in a thin insulating layer, separating bulk metallic conductors (with a mean free path l much larger than the size of the orifice). Actual point contacts usually are fabricated by pressing a metal needle on a metallic single crystal, followed by spot-welding. Point contacts in bulk doped semiconductors are fabricated by pressing two wedge-shaped specimens close together. Point contacts in a 2DEG cannot be fabricated by the same method, since the electron gas is confined at the GaAs-AlGaAs interface in the sample interior. The point contacts used in our studies are defined electrostatically by means of a gate on top of the heterostructure. In this way, short and narrow constrictions (QPCs of variable width comparable to the Fermi wavelength) in the 2DEG can be defined. There are another techniques that can be used to define constrictions of fixed width, such as etching. [9, 11]

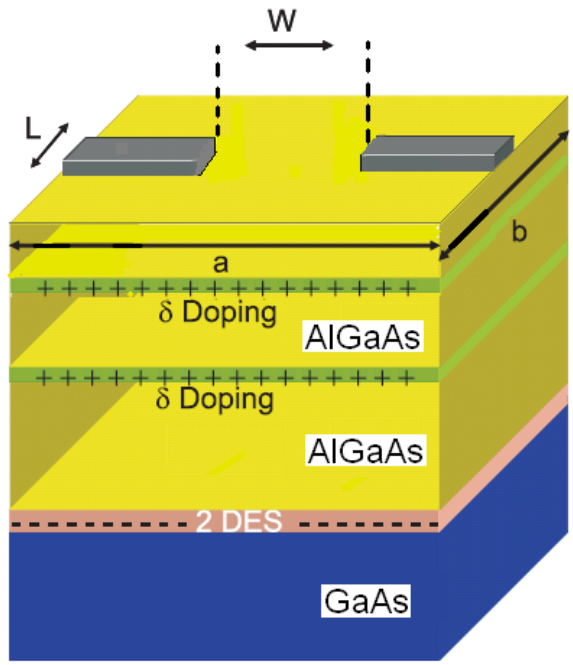

Figure 1.7.2: The GaAs-AlGaAs hetero-structure doped by silicon with 1500x1500x156 nm (*x*,*y*,*z*). The 2DES, donated by minus sings, is realized at 285 nm depth from the surface. The metallic gates are located at the surface with W = 562.5 nm separation. At zero bias, the electron density is determined by the number of donors. Charge distributions at different layers.

We simulated a hetero-structure which is shown in Figure 1.7.2 and for single and double QPC, the electron density profiles are calculated for different bias voltages. The system that we are interested in consists of several components, starting from the bottom, the substrate layer, 375 nm layer of GaAs growth over the substrate, an interface layer between GaAs and the upper AlGaAs layers, that is at 375 nm from the bottom or 285 nm from the surface, there is a 2DEG layer, two donor (δ) layers embedded into AlGaAs layer at 37.5 nm and 180 nm depth from the surface respectively. The density of charge of the upper donor layer is 1.7 x 10^{16} m^{-2} and the other donor layer has a 2.5 x 10^{15} m^{-2} charge density. The geometry we chose for the gates is a simple rectangle which has a width 500 nm and the distance between the gates is 562.5 nm. We used the same geometry and sizes for all QPCs here (single and double) as can be seen in the Figures 1.7.3 - 1.7.8. In Figures 1.7.3 - 1.7.8, the cross-sections of the electron density profiles and the potential distributions at the 2DEG for different gate voltages are shown. With increasing gate voltage, the charges under the gates are repulsed and depopulation of charges is observed under the gates. As can be seen from lower (b) panels of the Figures 1.7.3 – 1.7.8 which are for the potential distrubiton at the 2DEG, gate voltages creates potential wells and the charges are accumulated to these regions that has lower voltages.

The simulations will not go deeper, but further information about the gate defined QPCs can be found in the litarature and Refs. [9, 11].

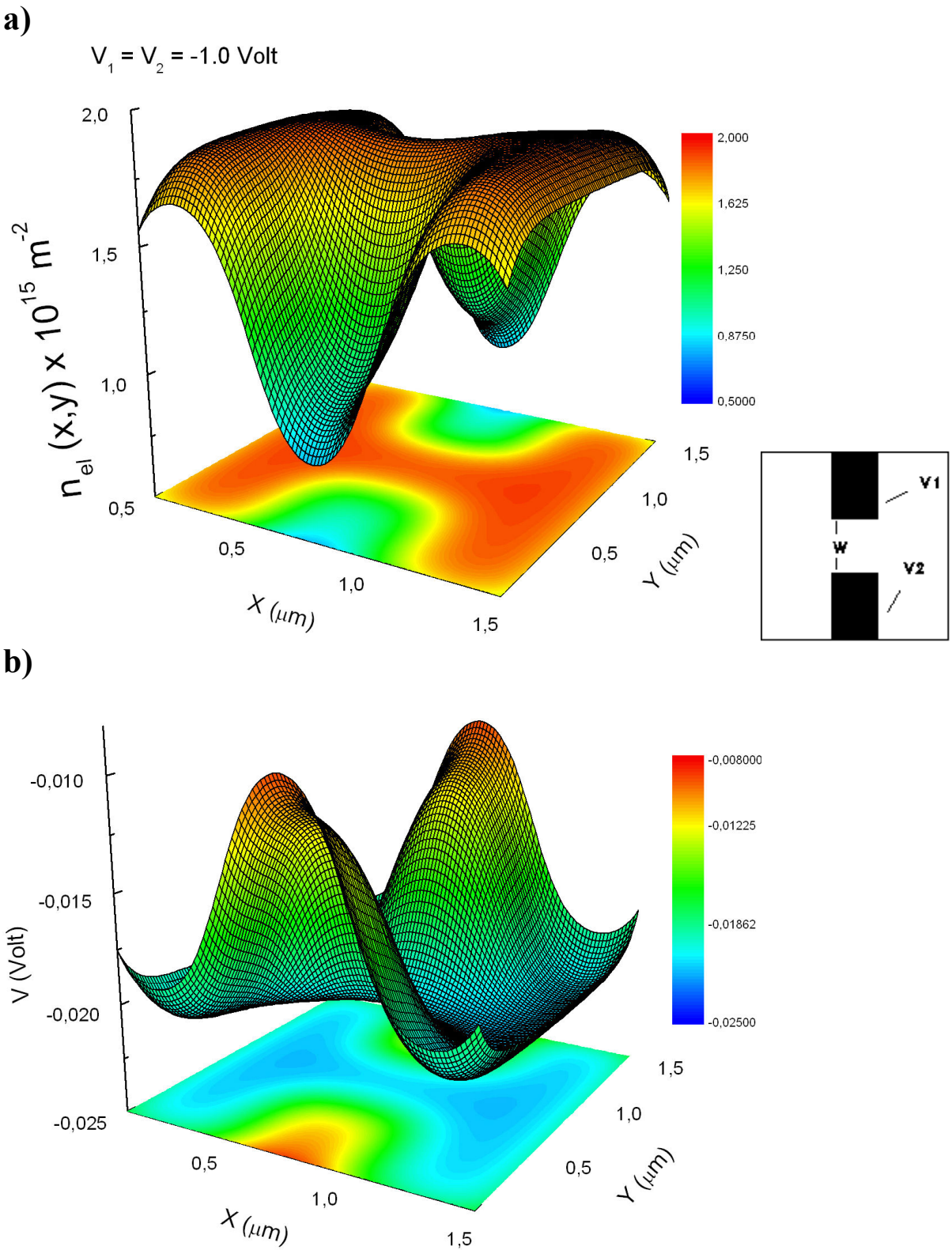

Figure 1.7.3: Simulation results of (a) the electron density distribution and (b) the potential distribution on the 2DEG for a single QPC. -1.0 Volt potential was applied to the gates; V_1 and V_2. The distance *W* between the gates is 562.5 nm.

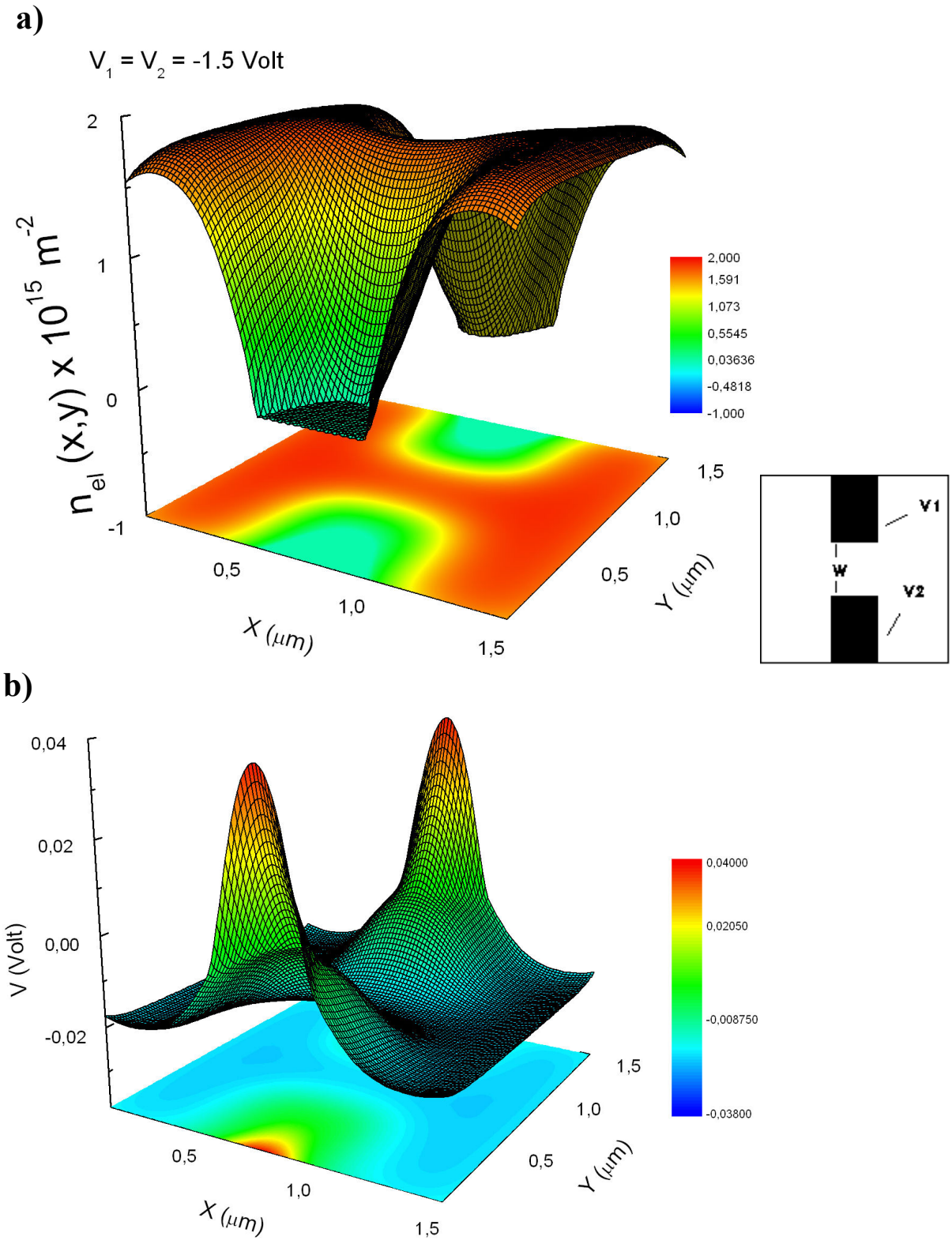

Figure 1.7.4: Simulation results of (a) the electron density distribution and (b) the potential distribution on the 2DEG for a single QPC. -1.5 Volt potential was applied to the gates; V_1 and V_2. The distance *W* between the gates is 562.5 nm.

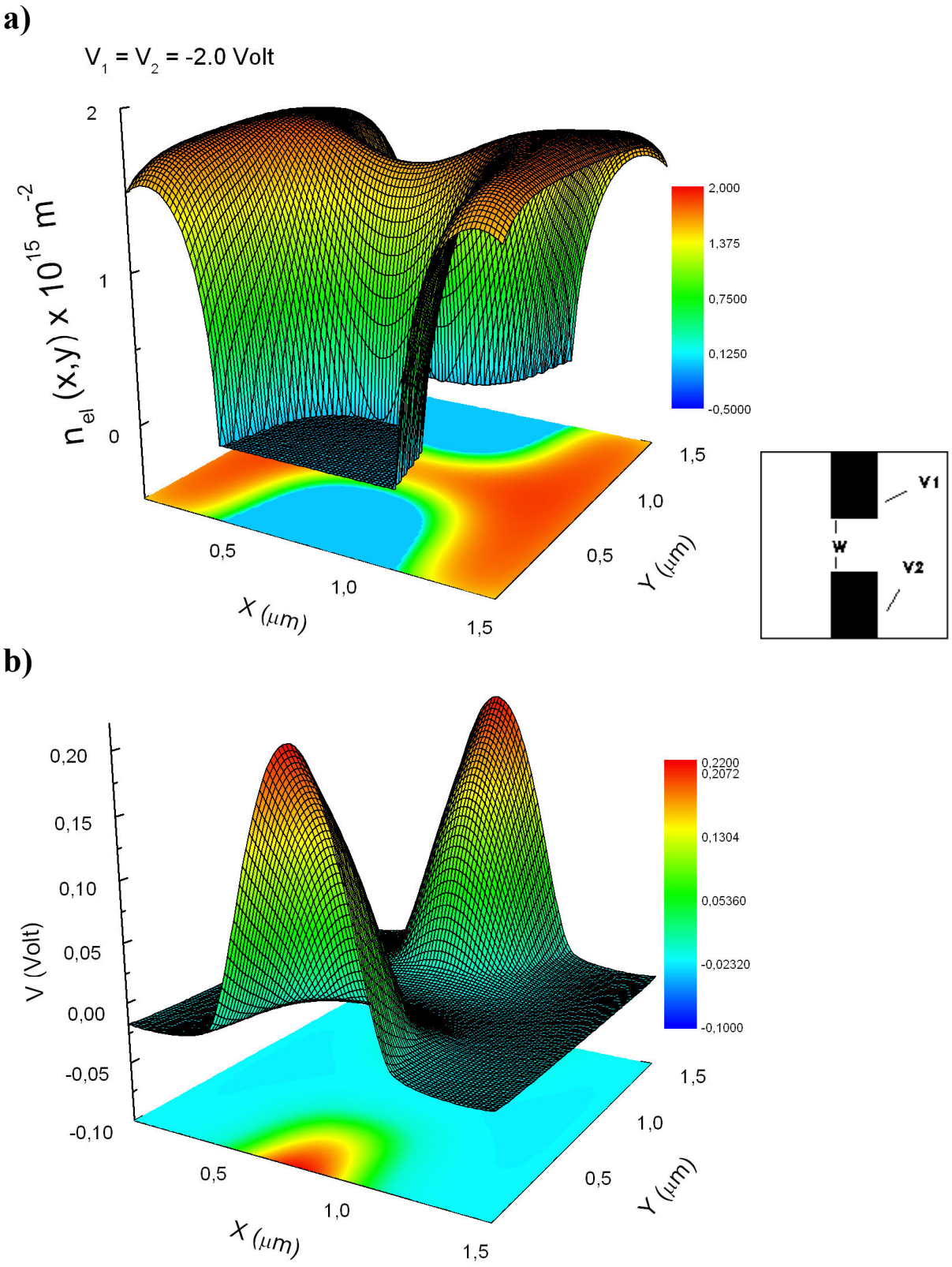

Figure 1.7.5: Simulation results of (a) the electron density distribution and (b) the potential distribution on the 2DEG for a single QPC. -2.0 Volt potential was applied to the gates; V_1 and V_2. The distance *W* between the gates is 562.5 nm.

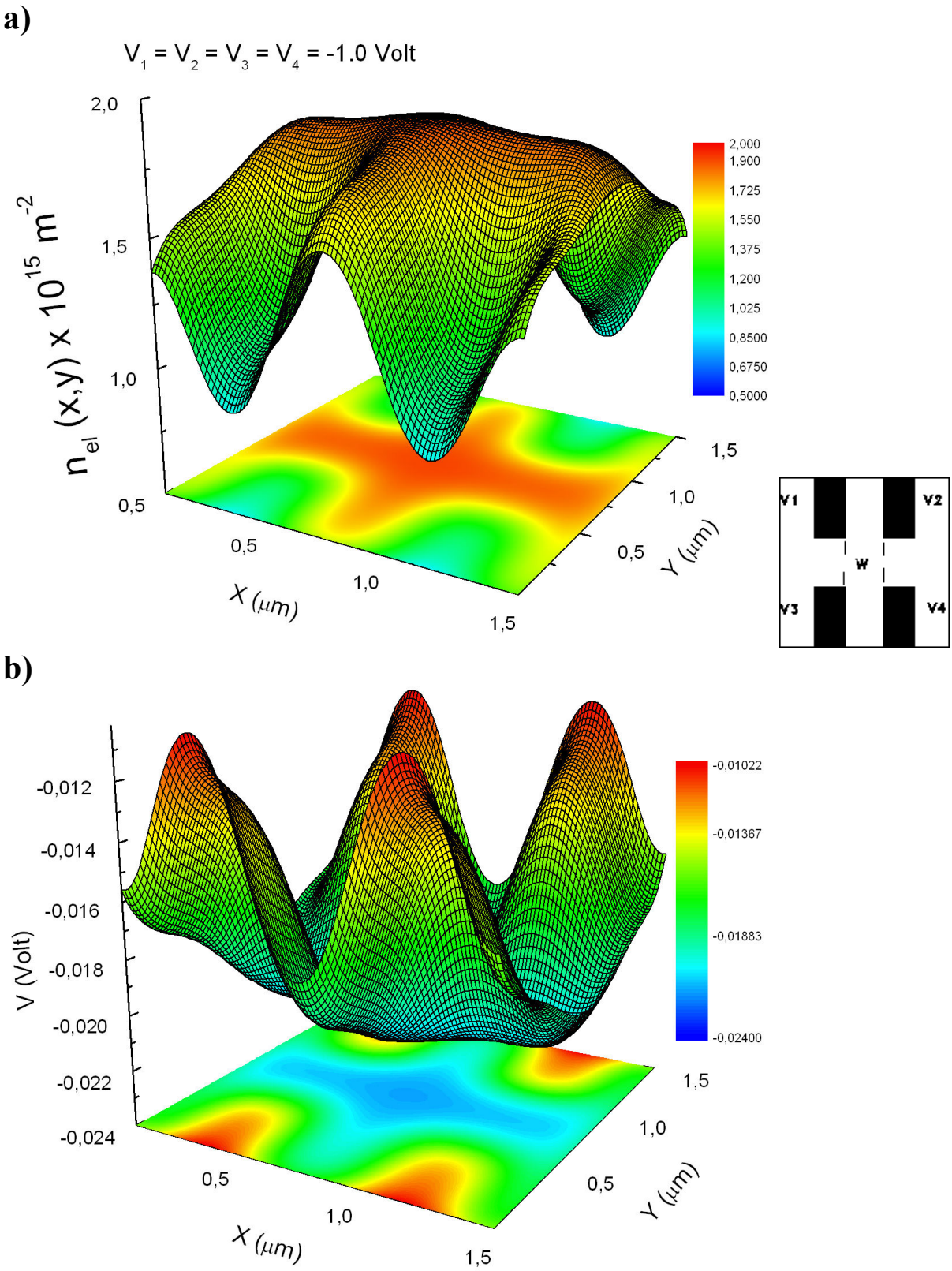

Figure 1.7.6: Simulation results of (a) the electron density distribution and (b) the potential distribution on the 2DEG for double QPC. -1.0 Volt potential was applied to the gates; V_1, V_2, V_3 and V_4. The distance *W* between the gates is 562.5 nm.

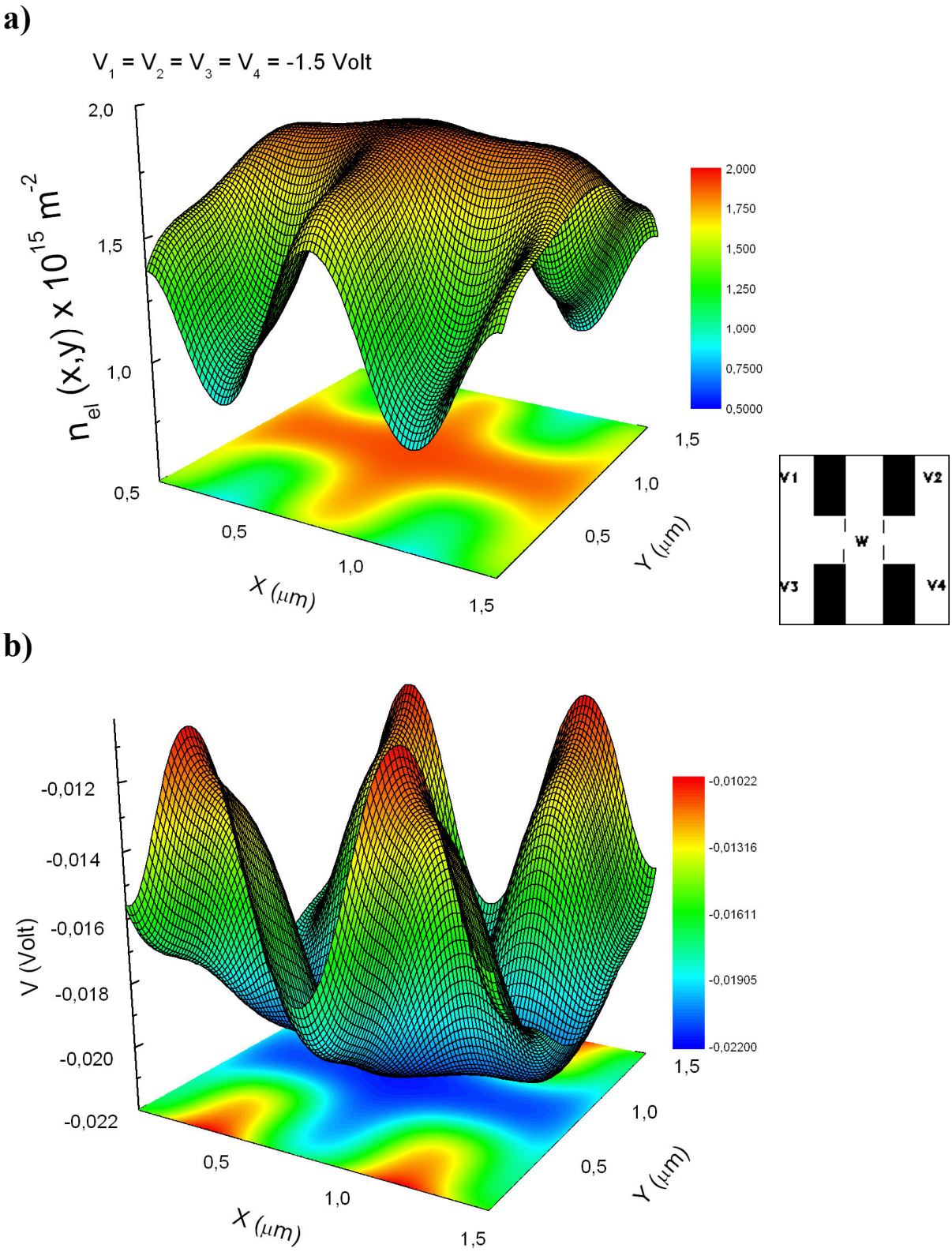

Figure 1.7.7: Simulation results of (a) the electron density distribution and (b) the potential distribution on the 2DEG for double QPC. -1.5 Volt potential was applied to the gates; V_1, V_2, V_3 and V_4. The distance *W* between the gates is 562.5 nm.

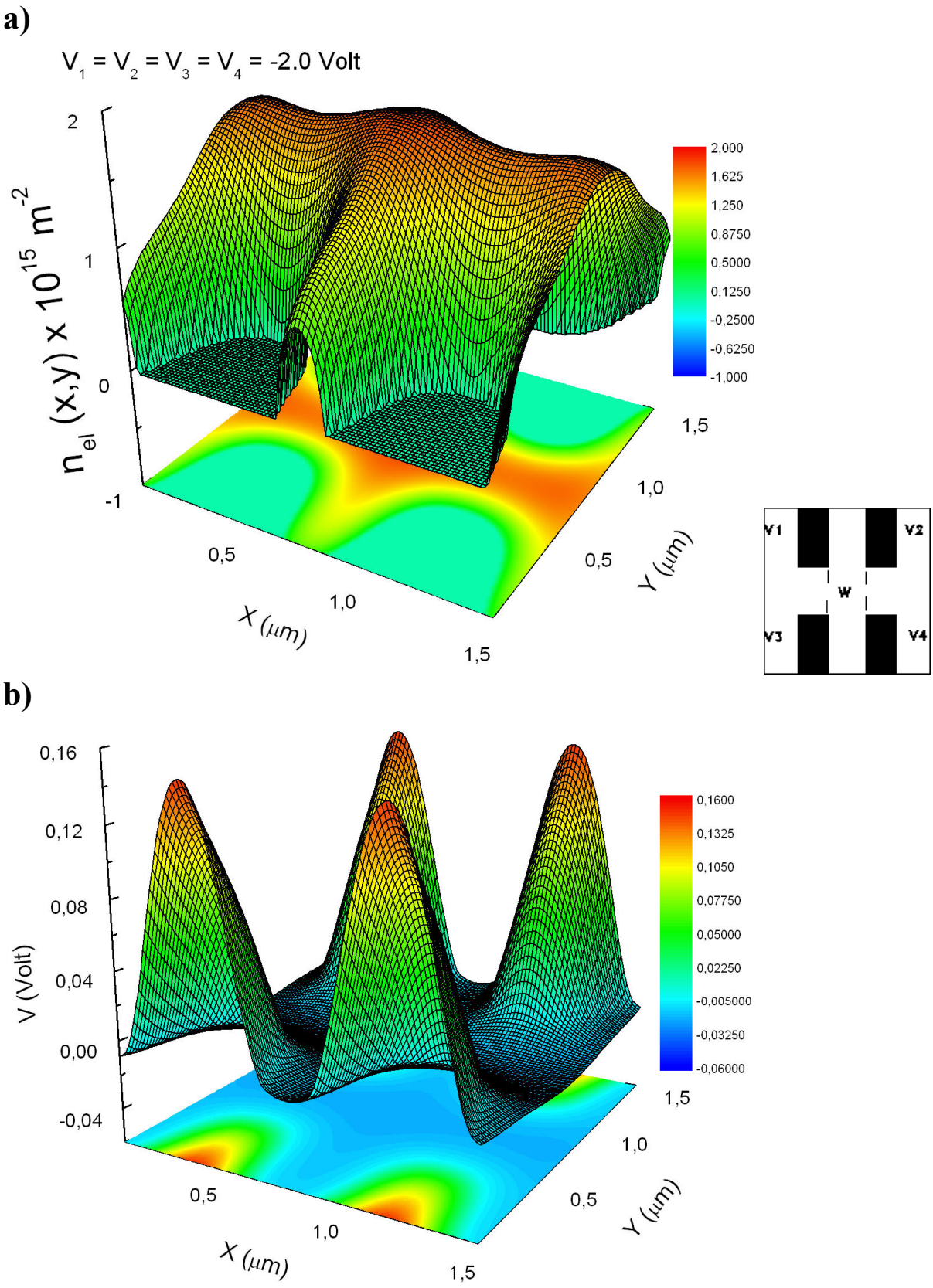

Figure 1.7.8: Simulation results of (a) the electron density distribution and (b) the potential distribution on the 2DEG for double QPC. -2.0 Volt potential was applied to the gates; V_1, V_2, V_3 and V_4. The distance *W* between the gates is 562.5 nm.

Chapter 2

Theoretical Background on Magnetism

2.1 Hall Effect

Edwin H. Hall, who was a 24-year-old graduate student, conducted an experiment and tried to determine whether the force experienced by a current carrying wire in a magnetic field was exerted on the whole wire or only on the moving electrons in it. Hall thought that if the current of in a fixed conductor is attracted by a magnet, the current should be drawn to one side of the wire and therefore the resistance experienced should be increased. He could not detect this extra resistance. However, he thought that the magnet must tend to deflect the current anyway, but it cannot do so. In this case he thought that there should be a state of stress in the conductor, the electricity pressing, toward one side of the wire. This stress should be a transverse voltage, which is known to be Hall voltage after E. Hall. We utilized Ref. [13, 14, 15] for this section.

The experiment is depicted in Figure 1. An electric field E_x is applied to a conductor extending in the x-direction and a current density j_x flows through it. A magnetic field $\vec{B}$ points in the z-direction. As a result of the Lorentz force, $-e\vec{v}\times\vec{B}$, the electrons tend to turn in to negative y-direction. However, the electrons cannot move much in the y-direction. When the electrons come closer to the side of the conductor, because of the potential difference occured between the sides, an electric field builds up in the y-direction that opposes the motion of the electrons. In equilibrium, this transverse field, Hall field, E_y will balance the Lorentz force, and current will flow only in the x-direction.

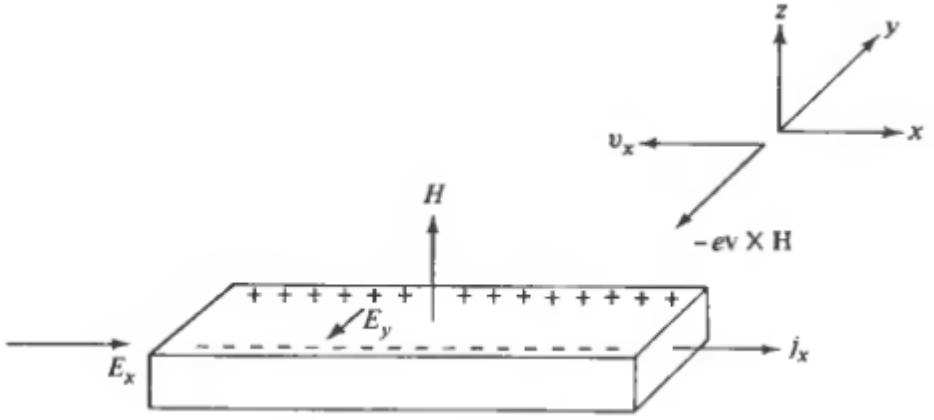

Figure 2.1.1: Schematic view of the Hall experiment.

There are two quantities of interest. One of them is the magnetoresistance (or transverse magnetoresistance. There is also a longitudinal magnetoresistance measured with the field paralel to the current.),

$$\rho(B) = \frac{E_x}{j_x}. \tag{2.1.1}$$

This is field independent. The other one is the size of the Hall field, E_y. It balances the Lorentz force, so it is proportional both to the applied field B, and to the current in the conductor j_x.

Hence, a quantity that is known as the Hall coefficient is defined,

$$R_H = \frac{E_y}{j_x B}. \tag{2.1.2}$$

Since the Hall field is in the negatice y-direction (Figure 2.1.1), R_H is negative. If the charge carriers were positive, then the sign of their x-velocity would be reversed, and therefore the Lorentz force would be unchanged. As a consequence the Hall field would determine the sign of the charge carriers. For Hall's original experiment, the sign of the charge carriers are negative as determined by Thomson. However, the Hall effect also showed that in some substances (especially p-type semiconductors), it is more appropriate to think of the current as moving positive 'holes' rather than negative electrons. There is a confusion usually occurs with the Hall effect that when holes move to the right is actually means that electrons move to the left or visa versa. So one expects the sign of the Hall coefficient is the same for both electrons and holes. This confusion can only be resolved by modern quantum mechanical theory of transport in solids.

To calculate the Hall coefficient and the magnetoresistance, the current densities j_x and j_y should be found firstly. The force on each electron is,

$$\vec{f} = -e(\vec{E} + \vec{v} \times \vec{B}). \tag{2.1.3}$$

And the momentum conservation equation for an electron is given as*,

$$\frac{d\vec{p}(t)}{dt} = -\frac{p}{\tau} + \vec{f}(t), \tag{2.1.4}$$

where the second term is frictional damping term due to electron's collisions.
Combining Eqs.(2.1.3) and (2.1.4) gives,

$$\frac{d\vec{p}(t)}{dt} = -(\vec{E} + \frac{\vec{p}}{m} \times \vec{B}) - \frac{\vec{p}}{\tau}. \tag{2.1.5}$$

* A derivation of this equation can be found in Chp.1 of Ref.[15]

For a steady state current, there is an independence of time and therefore the following equations can be written for p_x and p_y

$$0 = -e\vec{E}_x - \omega_c p_y - \frac{p_x}{\tau} \qquad (2.1.6.a)$$

$$0 = -e\vec{E}_y - \omega_c p_x - \frac{p_y}{\tau}, \qquad (2.1.6.b)$$

where $\omega_c = \frac{eB}{m}$.

To be able to get the current densities j_x and j_y, Eq.(2.1.6) is multiplied by $-ne\tau/m$ and remembering $\vec{j} = -ne\vec{v}$, current density components are introduced,

$$\sigma_0 E_x = \omega_c \tau \; j_y + j_x \qquad (2.1.7.a)$$

$$\sigma_0 E_y = -\omega_c \tau \; j_x + j_y, \qquad (2.1.7.b)$$

where σ_0 is the Drude model DC conductivity in the absence of magnetic field. The Hall field E_y is determined when the Hall potential is maximum, that is when Lorentz force balance is reached, that is the transverse current j_y is zero, hence setting j_y to zero in the Eq.(2.1.7.b) gives,

$$E_y = -\left(\frac{\omega_c \tau}{\sigma_0}\right) j_x = -\left(\frac{B}{ne}\right) j_x . \qquad (2.1.8)$$

Therefore the Hall coefficient, Eq.(2.1.2), is,

$$R_H = -\frac{1}{ne}. \qquad (2.1.9)$$

As it can be seen, the Hall coefficient does not depend on any parameter of the metal, except only the density of charge carriers. Therefore, a measurement of the Hall constant provides us the knowledge of charge carrier density. However, there is a problem about getting the knowledge of n from the measured Hall coefficients; they depend on magnetic field in general and also on temperature and the sample. This result seems unexpected, because the relaxation time τ does depend on the temperature and on the sample, and it does not appear in Eq.(2.1.9). At very low temperatures and high fields and if the pureness of the sample is high, the measured Hall coefficients approach a limiting value. This limiting value is the simple Drude result; Eq.(2.1.9).

2.2 Quantum Hall Effect

According to the Drude theory, the Hall resistivity decreases in inversely proportional to the electron density and it is independent of relaxation time, τ , in a weak magnetic field,

$$\rho_{xx} = \frac{m_e}{n_e e^2 \tau}, \qquad (2.2.1.a)$$

$$\rho_{xy} = \frac{B}{n_e e}, \qquad (2.2.1.b)$$

where m_e is the electron mass, n_e is the number of electrons and τ is the relaxation time which is defined as the mean time passed between two succesive collisions of an electron. However, the behavior in a strong magnetic field is quite different. In 1978, Wakabayashi and Kawaji conducted an experiment and they measured conductivity components, σ_{xx} and σ_{xy} of a Si-MOS sample. They found that there are regions where the diagonal conductivity becomes very small and the Hall conductivity (the inverse of ρ_{xy} in the Drude theory) approaches $n_e e/B$. In Figure 2.2.1, it can be seen that the results of an experiment by Wakabayashi and Kawaji. [9, 16, 17, 22]

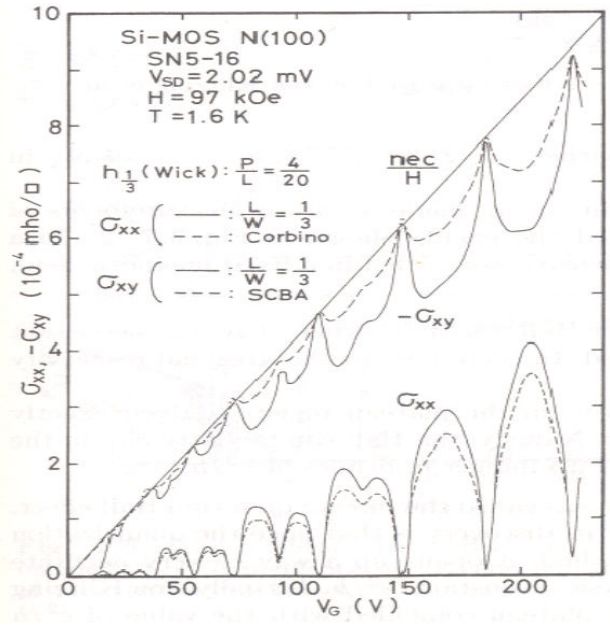

Figure 2.2.1: The Hall and longitudinal conductivities measured by Wakabayashi and Kawaji. [11]

According to Eq.(2.2.1.b), the Hall resistance is expected to change linearly with the magnetic field B. However, in 1980, von Klitzing et al. made very accurate measurements for resistivity and he found that, at high magnetic fields and low temperatures (about 1 K), the

Hall resistance did not change linearly with the field. He saw in the plot (Fig.2.2.2) a series of "stair steps" like plateaus. In these constant Hall plataue regions in Hall resistivity, the longitudinal resistivity becomes so small that it vanishes almost. They also showed that the Hall resistivity in the plataue region is given exactly by h/e^2 devided by an integer, that is the Hall conductivity σ_{xy} in the plataue region is quantized into integer multiples of e^2/h. Hence, this phenomenon was called the integer quantum Hall effect.

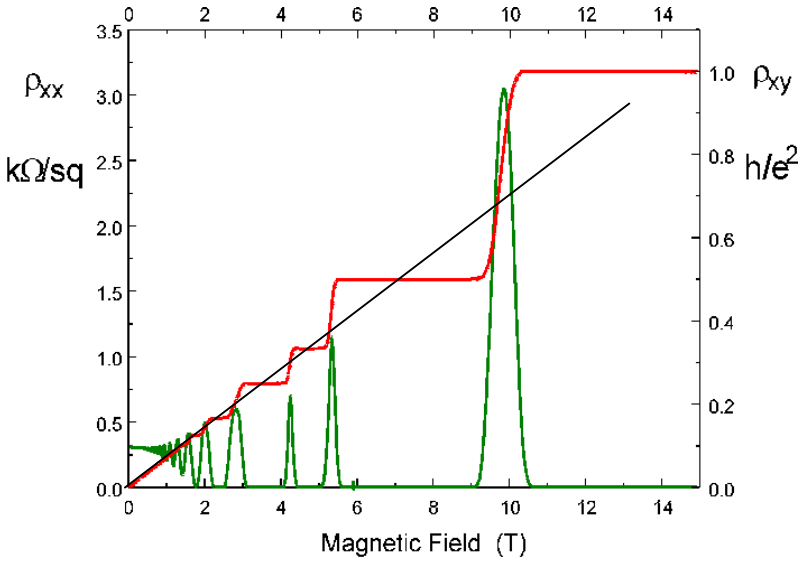

Figure 2.2.2: There is shown the integer quantum Hall effect in a GaAs-GaAlAs heterojunction, recorded at 30 mK. The straight black line shows the expected classical behavior. [22]

In two dimension, there are circular paths in which (classical) electrons are forced to move by the field on them. Quantum mechanical nature prevents the electron orbits from overlapping. As the field increases, the orbital radius decreases, permitting more orbits to bunch together on one side of the material. The changes in orbital motion occur suddenly, corresponding to the plataues, because of the quantization of the orbital motion of the electrons, that is only certain orbits being allowed. The energy levels of these quantized orbitals take on discrete values, called Landau levels,

$$E_n = \hbar\omega_c(n+1/2)\,, \qquad (2.2.2)$$

where $\omega_c = eB/m$ is the cyclotron frequency. For strong magnetic fields, each Landau level is highly degenerate (i.e. there are many single particle states which have the same energy E_n). For strong magnetic fields, each Landau level can have so many states that all of the free electrons in the system sit in only a few Landau levels; it is in the regime that the quantum Hall effect is observed.

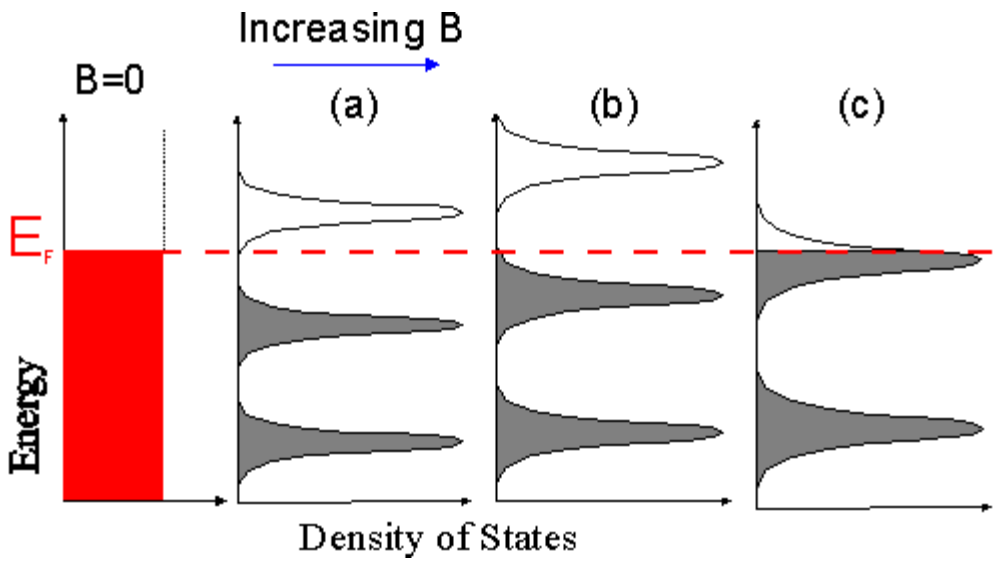

F

Figure 2.2.3: In the absence of magnetic field the density of states in 2D is constant as a function of energy, but in field the available states clump into Landau levels (LL) separated by the cyclotron energy, with regions of energy between the LLs where there are no allowed states. As the magnetic field is swept the LLs move relative to the Fermi energy. When the Fermi energy lies in a gap between LLs electrons can not move to new states and so there is no scattering. Thus the transport is dissipationless and the resistance falls to zero. [22]

The quantized Hall resistance h/e^2 is known to a precision of less than 1 part in 10^{10}, so the quantized Hall effect is used for a new standard for resistance. [16]

2.3 Edge States

In a magnetic field, the electrodynamics of a two-dimensional system is different from the three-dimensional case. In the three-dimensional case, the linearly varying wiving potential inside the sample is produced by a surface charge at the sample edges. So, in a magnetic field the surface charge which gives rise to the Hall voltage cancels the Lorentz force on a homogeneous current density in the sample. In contrast, in a two-dimensional system neither a surface charge nor a redistribution of the charge density in the bulk of the 2DEG can produce a linearily varying potential across the system. A nonlinear Hall field has therefore to exist in a two-dimensional sample. [18, 19, 20]

The edge of a system can be thought as a confining potential and the details of the electron state depend on the form of the potential. The state of the electron can be found from the solution of the Schrödinger equation, where the boundary conditions are fixed by the confinement potential. In the presence of an external magnetic field, common results show

that the energy of an electron state increases as the state approaches the edge. The motion of an electron at the edge can be imagined as if in classical mechanics as a skipping orbit along the edge. Figure 2.3.1 shows these classical trajectories of an electron moving in a magnetic field at the edge of a sample.

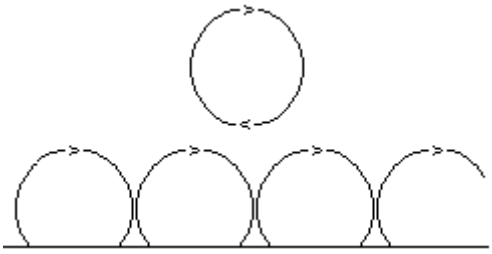

Figure 2.3.1: Classical trajectories (skipping orbits)
of electrons moving along the edge of a sample in magnetic field.

The Hamiltonian of a 2DEG in a magnetic field perpendicular to the 2DEG is,

$$H = \frac{1}{2m}\left[(p_x - eB_y)^2 + {p_y}^2\right] + V(x,y), \qquad (2.3.1)$$

given the vector potential $\vec{A} = (-zB_y, 0, 0)$, in Landau gauge. The hamiltonian is not separable for an arbitrary potential $V(x,y)$. If $V(x,y)$ depends only on the y coordinate the Hamiltonian is separable with the wavefunction,

$$\psi_{nk}(x,y) = e^{ikx}\varphi_{nk}(y), \qquad (2.3.2)$$

hence we get the eigenvalue problem ,

$$E\varphi_{nk} = \left(-\frac{\hbar^2}{2m}\frac{\partial^2}{\partial y^2} + \frac{m}{2}\omega_c^2(y_0 - y)^2 + V(x,y)\right)\varphi_{nk}, \qquad (2.3.3)$$

where $\omega_c = eB/m$ is the cyclotron frequency, m is the effective mass of the electron and $y_0 = -kl_c^2$, $l_c = \sqrt{\hbar/eB}$ is the magnetic length. The parameter y_0 gives the center of the cyclotron orbit. For a vanishing potential $V(y) = 0$, the eigenfunctions $\varphi_{nk}(y)$ are the harmonic oscillator functions,

$$\varphi_{nk}(y) = N\exp[-(y - y_0)^2/2l^2]H_n[(y - y_0)/l_c], \qquad (2.3.4)$$

where H_n is the Hermite polynomials, N is the normalization and the energy eigenvalues are the ones for the harmonic oscillator which are,

$$E_n = \hbar\omega_c\left(n+\frac{1}{2}\right). \qquad (2.3.5)$$

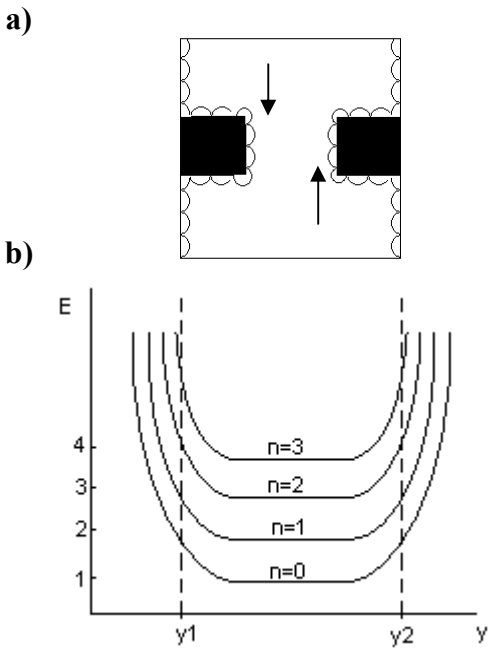

Figure 2.3.2: a) Electron motion in skipping orbits at the edge states in 2DEG b) energy spectrum of a 2DEG in a magnetic field with confining potentials at the edges, y1 and y2.

At the edges, for a non-vanishing potential, the energy eigenvalues increase near the edges and become k dependent. The energy levels for some Landau quantum numbers as a function of y_0 can be seen in Figure 2.3.2. These states which have a raised energy and cause electron motion along the edge are called "edge states". In Figure 2.3.2, states can be observed beyond the sample edges defined by y1 and y2. In the classical picture of skipping orbits, the centre of the cyclotron orbit can be outside of the sample, and the same effect holds for the quantum-mechanical picture. However, in both cases, the centre of mass of the electrons at the edges stays inside the sample giving rise to an increase in carrier concentration near the edge of the sample.

The current-carrying states belonging to one Landau quantum number at one edge are often called edge channels.

2.4 Local Ohm's Law

To produce an electric current in a circuit, a potential difference is required. The potential induces an electric field that will force the charges to flow. Usually, the current density $\vec{j}$ is proportional to the force per unit charge, $\vec{f}$:

$$\vec{j} = \sigma \vec{f} \,, \tag{2.4.1}$$

where the proportionality factor σ is the conductivity which depends on the material or the medium. [21]

The force $\vec{f}$ is usually an electromagnetic force, so the Eq.(2.4.1) becomes,

$$\vec{j} = \sigma(\vec{E} + \vec{v} \times \vec{B}) \,. \tag{2.4.2}$$

Since the velocity of the charges is too small, the second term on the right hand side of the Eq.(2.4.2) can be neglected. Hence, the equation becomes,

$$\vec{j} = \sigma \vec{E} \,. \tag{2.4.3}$$

This is the Ohm's law. Since any assumptions about the shape of the body is not required, Ohm's law in this vector form is valid at any point of a body. Suppose an arbitrarily shaped body with current flowing through it, if we look at the coordinates (x,y,z) without changing the flow of the current, we find that the local current density and the local field strength obey the Eq.(2.4.3) given above locally, [21]

$$\vec{j}(x,y,z) = \sigma(x,y,z)\vec{E}(x,y,z) \,.$$

There is no good reason that tells why $\vec{j}$ is always parallel to $\vec{E}$. This means that for the most general case σ is not a scalar quantity, but a tensor; $\sigma = \sigma_{ij}$. Then the Ohm's law can be rewritten as following,

$$\begin{pmatrix} j_x \\ j_y \\ j_z \end{pmatrix} = \begin{pmatrix} \sigma_{xx} & \sigma_{xy} & \sigma_{xz} \\ \sigma_{yx} & \sigma_{yy} & \sigma_{yz} \\ \sigma_{zx} & \sigma_{zy} & \sigma_{zz} \end{pmatrix} \begin{pmatrix} E_x \\ E_y \\ E_z \end{pmatrix} . \tag{2.4.4}$$

This is the most general version of Ohm's law. For anisotropic inhomogeneous materials the tensor have to be taken, and its components depend on the coordinates. In two dimension, the above equation reduces to,

$$\begin{pmatrix} j_x \\ j_y \\ 0 \end{pmatrix} = \begin{pmatrix} \sigma_{xx} & \sigma_{xy} & 0 \\ \sigma_{yx} & \sigma_{yy} & 0 \\ 0 & 0 & 0 \end{pmatrix} \begin{pmatrix} E_x \\ E_y \\ 0 \end{pmatrix} . \tag{2.4.5}$$

$$\Longrightarrow \quad \begin{pmatrix} j_x \\ j_y \end{pmatrix} = \begin{pmatrix} \sigma_{xx} & \sigma_{xy} \\ \sigma_{yx} & \sigma_{yy} \end{pmatrix} \begin{pmatrix} E_x \\ E_y \end{pmatrix} . \tag{2.4.6}$$

Chapter 3

Equilibration

3.1 Equilibrium

In chapter 1, we only obtained the potential and the electron density distributions in the case of electrostatic equilibrium. This means that all the electrons have effectively zero force acting on them. The next step is to include the effect of quantizing magnetic field and again obtain electrostatical equilibrium, which requires finding the vanishing total force also including the Hall effect.

In the following, we present similar numerical results considering quantum point contacts and also the formation of skipping orbits (incompressible strips) without an external current. In other words, the number of forward moving electrons is equal to the number of backward moving electrons, hence the total current vanishes and equilibrium is established.

In Figure 3.1.1, we show the spatial distribution of electron density (a) and potential distributions. The black regions (strips) corresponds to incompressible strips, i.e. skipping orbits. Here, the electrons within the incompressible strips reside in the second Landau level (n=1). It is common to describe dimensionless quantity, the filling factor ν . It is given as,

$$\nu = \frac{2E_f}{\hbar\omega_c}.$$

Hence, this dimensionless number gives the occupation of Landau levels. One can imagine that the second orbital of the quantized cyclotron motion is occupied. It is straightforward to see that once the magnetic field is changed, the location of skipping orbits will also change as shown in the Figures in this section. Notice that on the right hand side of the Figure 3.1.1.a, the electrons are moving in positive y direction, meanwhile on the left hand side, electrons move on the opposite direction so that the total current is zero and our system is in equilibrium.

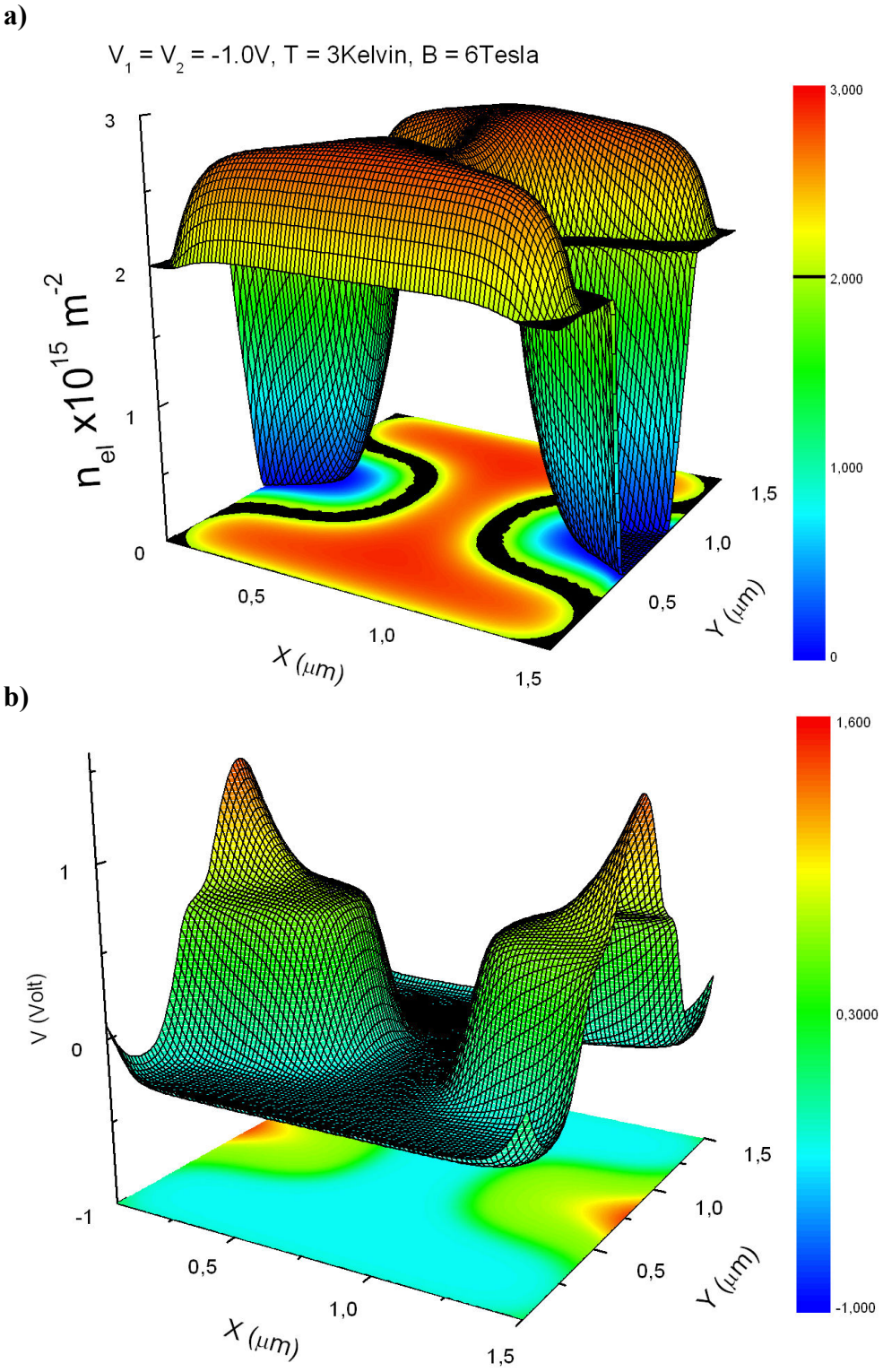

Figure 3.1.1: a) Electron density distribution and b) potential distribution for the 2DEG calculated for a single QPC.

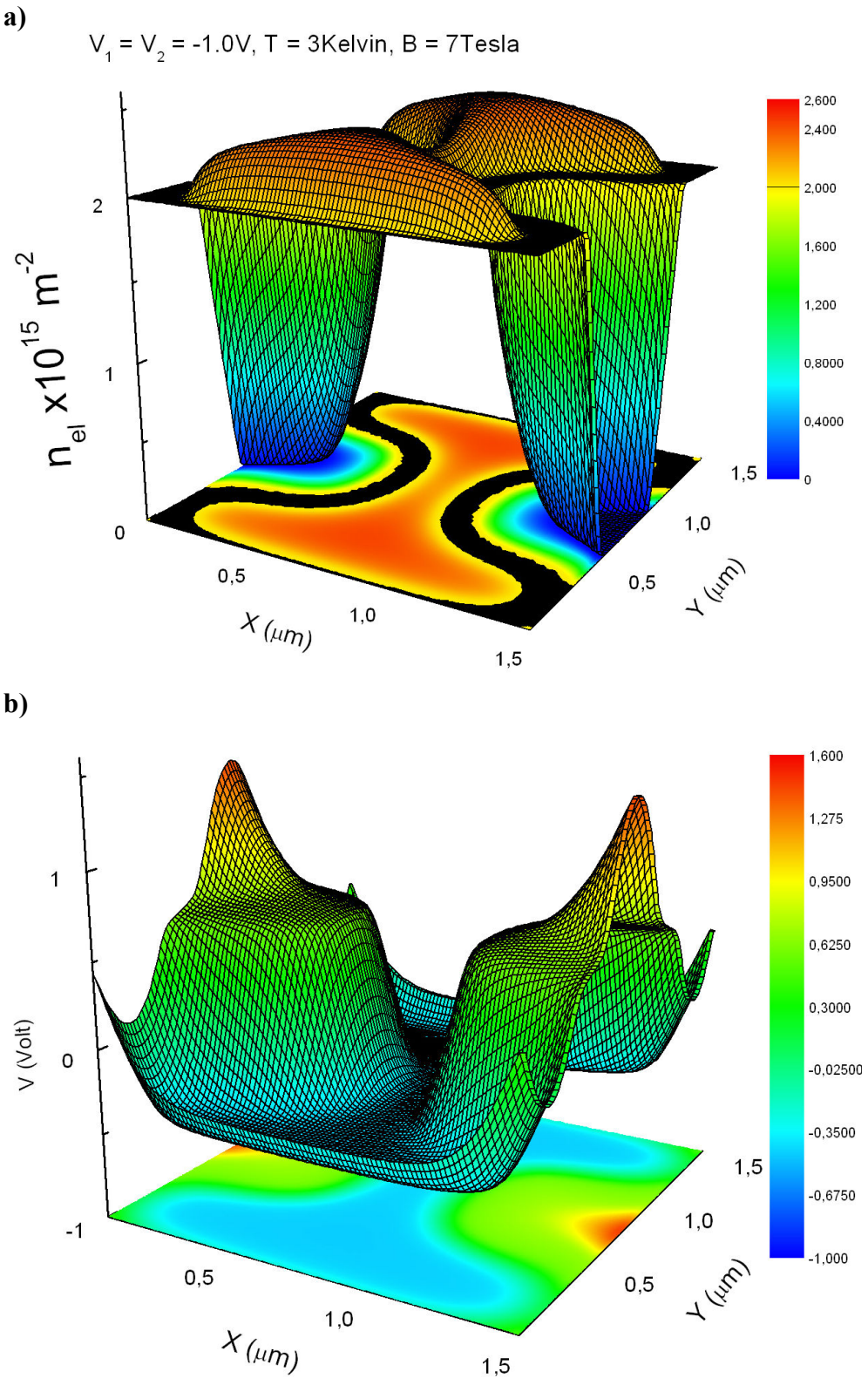

Figure 3.1.2: a) Electron density distribution and b) potential distribution for the 2DEG calculated for a single QPC.

3.2 Non-equilibrium

To disturb equilibrium, one imposes an external potential difference between x = 0 μm and x = 1.5 μm (x coordinate is given for just the figures in this section. In the figures in other sections, the coordinates are given different as you can notice). Therefore, finite number of electrons flow through the device. The current distribution is showed in Figure 3.2.1.b. It is apparent that the current traces the spatial distribution of incompressible strips. This is due to the fact that the longitudinal resistivity vanishes at incompressible strips. As we have seen previously, altering the magnetic field will change the current distribution also. This is seen in Figures 3.2.2 and 3.2.3.

It is worth to note that the magnetic field does not change only the positions, but also the thicknesses of the current carrying edge states (channels). In any case, the left and right edge channels are decoupled due to the compressible bulk. Therefore, an equilibration process cannot take place. However, for certain magnetic fields, these channels can come to a close proximity where the bulk becomes incompressible. Then one could expect equilibration of left and right channels which we will be investigating in the next section.

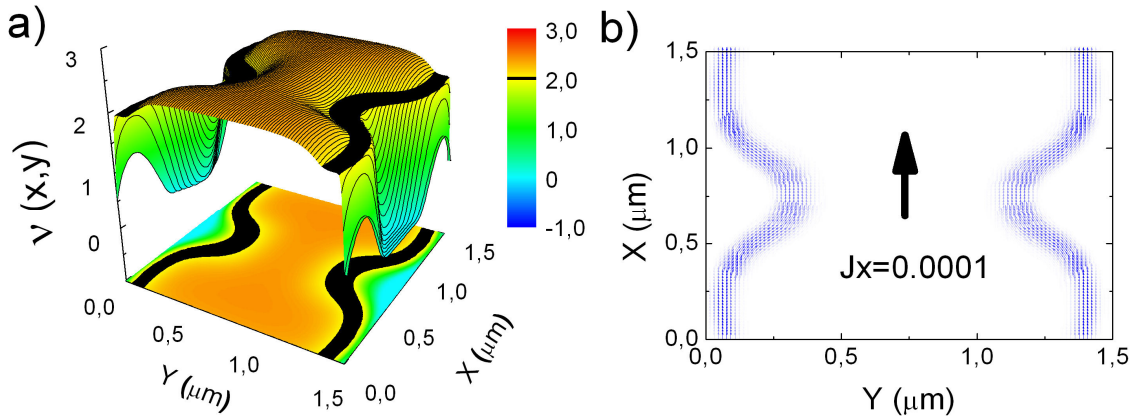

Figure 3.2.1: Electron density profile for a single QPC. B = 6 T. T = 5 mK. -1.5 Volt potential was applied to the gates.

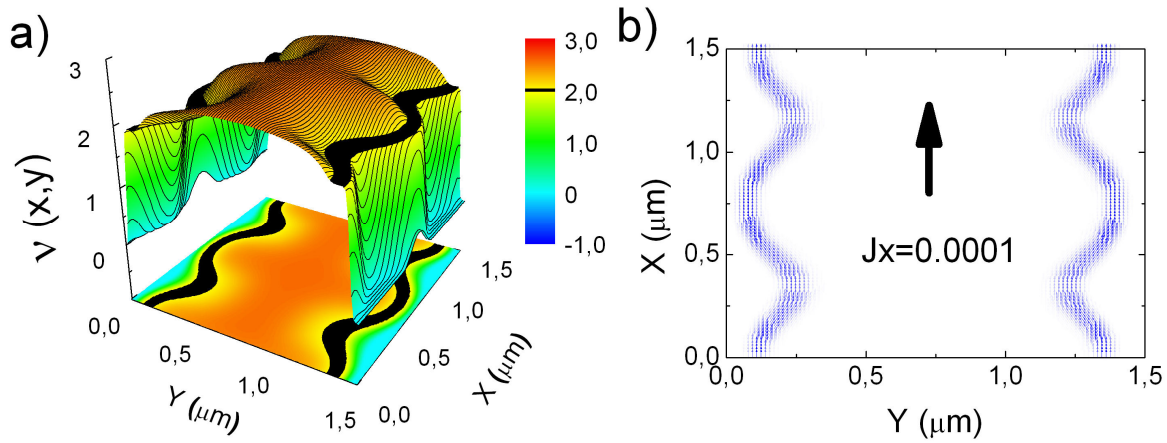

Figure 3.2.2: Electron density profile for a double QPC. B = 6 T. T = 5 mK. -1.5 Volt potential was applied to the gates.

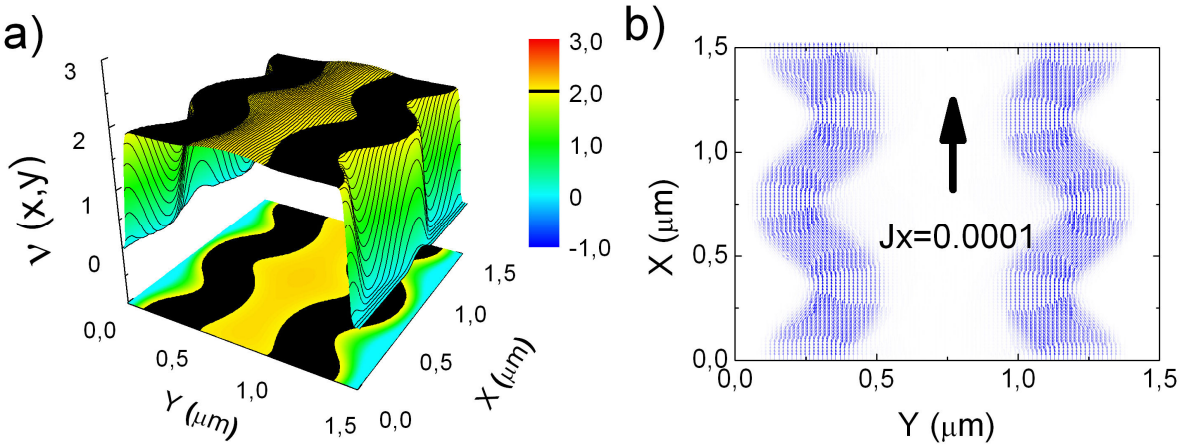

Figure 3.2.3: Electron density profile for a double QPC. B = 7 T. T = 5 mK. -1.5 Volt potential was applied to the gates.

3.3 Equilibration

As discussed previously, magnetic fields can generate an equilibrated edge transport. Alternatively, one can change the geometry or applied gate potentials to generate an incompressible bulk where equilibration can take place.

Here we show as a singular case, the formation of an incompressible bulk in Figure 3.3.1.a. The currents flowing from the bulk is equilibrated, hence one cannot distinguish between the left or the right incoming electrons.

Investigation of equilibration depending on the given system parameters requires further numerical efforts. However, in Figure 3.3.2, we present schematically other possible configurations which we expect to have.

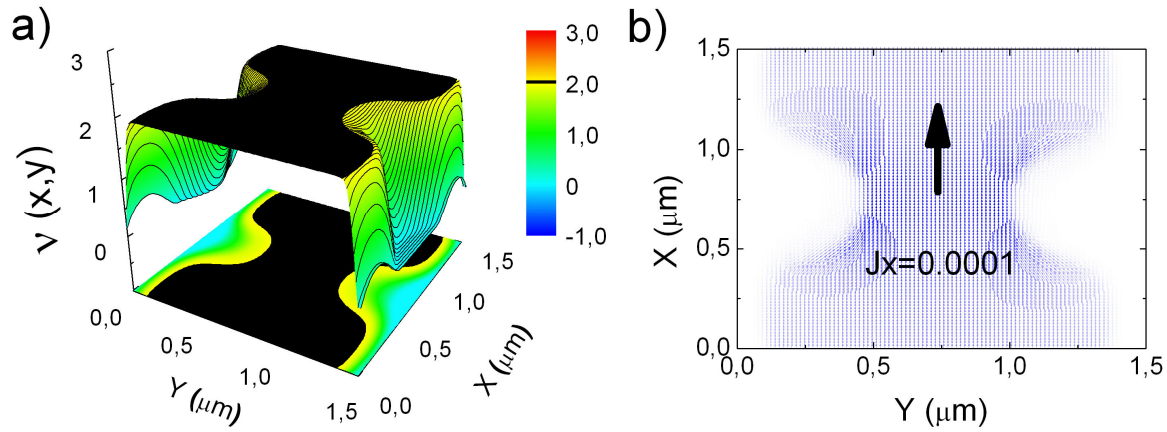

Figure 3.3.1: Electron density profile for a single QPC. B = 7 T. T = 5 mK. -1.5 Volt potential was applied to the gates.

In Figure 3.3.2.a, the equilibration length, L, strongly depends on the applied gate voltage at a fixed magnetic field as can be seen from (b). Once voltages applied to the gates, the edge states are repelled from the quantum point contact and the equilibration length, L, can be reduced to as small as a single point. Meanwhile, increasing the magnetic field can either enlarge the strip widths or even create a bulk incompressible region where equilibration length can be as large as the sample length.

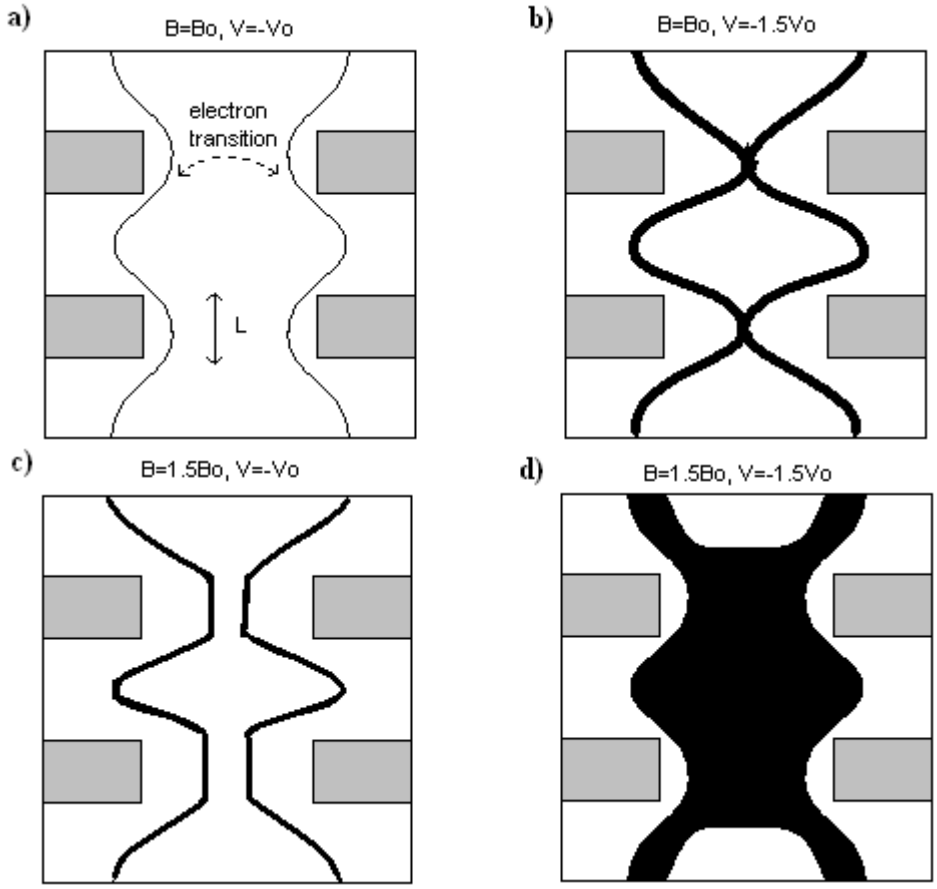

Figure 3.3.2: Some possible configurations are given schematically.

Chapter 4

Conclusion

In this report of my final year project, we presented the preliminary version of our calculations where the Poisson's equation is solved self-consistently. We have investigated a particular quantum device, namely the quantum point contact, which is defined by metalic gates deposited on the surface of the heterostructure. Also taking into account the gates, material properties of the heterostructure, the electron gas and imposing relevant boundary conditions, we obtained the electron density and potential distribution profiles analyzing gate voltage dependency. In a further step, we included the effect of quantizing magnetic field starting from the classical Hall effect. We briefly discussed the skipping orbit picture where the current is carried. In the absence of an external current, i.e. in equilibrium, we show that the number of forward moving electrons is equal to the number of backward moving electrons. In the presence of external current, utilizing the local Ohm's law, we investigated the current distribution near the quantum point contacts. In this non-equilibrium case, if the current carying channels are far apart, equilibrium is not restored. However, by manipulating the gate potentials and magnetic field, we onserved that equilibration can take place, where left incoming or right incoming electrons cannot be distinguished.

In our future work, we plan to proceed with further calculations of equilibration conditions. In particular, we plan to address the quantitative description of the equilibration length depending on the geometry, magnetic field and the heterostructure paramaters.

Appendix A

Data Files

In the following parts, the input files that were used for the calculations are given.

A.1 Input File For Est3D

Here I gave an input file used for a single quantum point contact. -1.0 gate voltage applied to the gates. The name of the QPC is ‘qpc1’ whose pattern profile is defined in the corresponding gates.srf file.

```
%% estatic parameter file
%% NB! grid spacing needs to be the same in all dimensions in order
%% for the equations used to hold (in given accuracy)

%% SETUP DIMENSIONS

 %  NX0   NY0   NZ0    LX       fhY     fhZ
SYS_PARAS = [  128   128   137   2.0E-6   1.   0.4762 ]

          %   LR    PL    PR    PC   trans
VGATES    = [ -3.2  -2.5  -2.5  -4.5   -.75  ]

BDR_FILE  = {
% FILE NAME -- SHIFT_X,Y,Z - bXY - bZ --------------------------------
  'gates.srf'        0 0 0    6    6      'file' % user structure file

% VARNAME -- SHIFT_X,  Y,  Z - [VQ]   VALUE - DESCRIPTION --
 'qpc1'            0   0  90   'V'    -1.0   'disa gate'  % gate
}

MOUT_DXY  = 0
LOG_ZDIST = 1  % logarith. zdist for PISLk

% ------------------------------------------------------------------------------ %
% ------------------------------------------------------------------------------ %

QDOT_LABEL = 'dot';
```

```
% NB! *<label>[0-9][lrab] will be linked to *G[0-9]p[lrab]

ISLANDS  = {
%% VARNAME --- I1  J1  K1 -- I2  J2  K2 -- [VQ] - VALUE ----------
 'dielec'     3   3   3   124 124  92     'D'   12.0
 'surf'       6   6  91   121 121   ~    'VO-'  -0.75
 'donors1'    6   6  69   121 121   ~    'C2'   2.50E15
 'donors2'    6   6  86   121 121   ~    'C2'   1.70E16
 '2DEG'       6   6  53   121 121   ~    'VO-'   0.0

}

% ------------------------------------------------------------------------------- %

QV_SERIES = [
 % VSET -- V2 --- V3 --- V4 -- --- N - % N = # intervals
    0.   +0.1     0      0  ~     3   %
 % ISL-IDX FLAGS[01] LOG -- V1 -- V2 - % - ------------------------------
 '2DEG'    ~  ~     Z      ~     ~   % 2DEG
 'lo_surf'  ~  Q     Y      ~     ~   % shallow etched surface (pioda)
 'tip'      X  ~     Y     V1    V2   % transition gate
]; %% ---------------------------------------------------------------------------

QP_SERIES = [
 % ISL-IDX FLAGS[01] LOG [FILE:]VAR - SHIFT_[XYZ] - --------------
 '2DEG'    ~  ~     Z         ~     ~   ~   ~   % 2DEG
 'surf2'   ~  Q     Y         ~     ~   ~   ~   % Qconst after shallow etch
 'tip'      X  ~     Y     'tpos'  +10   0   0   % parabolic tip
]; %% ---------------------------------------------------------------------------

% ------------------------------------------------------------------------------- %
% ------------------------------------------------------------------------------- %
```

List of Figures

1.4.1 The simple Euler method……...6
1.4.2 The modified Euler method……....8
1.4.3 The improved Euler method……...8

1.6.1 Shematic view of the structure in grid dimensions.....14

1.7.1 Quantum tunneling through a potential barrier……...…….....16
1.7.2 GaAs-AlGaAs hetero-structure…….....18
1.7.3 Electron density and potential distributions for single QPC…….…….....19
1.7.4 Electron density and potential distributions for single QPC…….…….....20
1.7.5 Electron density and potential distributions for single QPC…….....…..21
1.7.6 Electron density and potential distributions for double QPC……..….22
1.7.7 Electron density and potential distributions for double QPC……....23
1.7.8 Electron density and potential distributions for double QPC……....24

2.1.1 Schematic representation of The Hall experiment…..……..…….....25
2.2.1 The Hall and longitudinal conductivities by Wakabayashi and Kawaji.……...28
2.2.2 The integer quantum Hall effect in a GaAs-AlGaAs heterojunction.……....29
2.2.3 Density of states vs. enegy in 2D……..30
2.3.1 Skipping orbits of electrons moving along the edge of a sample…...…….....30
2.3.2 Energy spectrum of a 2DEG in a magnetic field……...……..…31

3.1.1 Electron density and potential distributions for single QPC ……...……..…37
3.1.2 Electron density and potential distributions for single QPC ……...……..…37
3.2.1 Electron distribution profile (with current)……...…….…39
3.2.2 Electron distribution profile (with current)……...…….…40
3.2.3 Electron distribution profile (with current)……...…….…40
3.3.1 Electron distribution profile (with current)……...…….…41
3.3.2 Some possible configurations for the equilibration……...……...…….…41

References

[1] D. J. Griffiths, *Introduction to Electrodynamics* (3th ed.) (Prentice Hall, 1999)

[2] W. E. Boyce, R. C. DiPrima, *Elementary Differential Equations and Boundary Value Problems* (7th ed.) (John Wiley & Sons, 2001)

[3] http//:mathworld.wolfram.com/BoundaryConditions.html

[4] P. L. DeVries, *A First Course in Computational Physics* (John Wiley & Sons, 1994)

[5] S. E. Koonin, *Computational Physics* (Benjamin, 1986)

[6] S. E. Koonin, D. C. Meredith, *Computational Physics – Fortran Version* (AW, 1990)

[7] J. M. Thijssen, *Computational Physics* (Cambridge University Pres, 1999)

[8] Francis J. Scheid, *Schaum's Outlines – Numerical Analysis* (Mc Graw-Hill, 1988)

[9] S. Arslan, *Image Processed Modelling of Quantum Point Contacts* (Master's Thesis) (Technische Universitat München, 2008)

[10] The program manual of Est3

[11] S. Arslan, E. Çiçek, D. Ekşi, S. Aktaş, A. Weichselbaum, A. Sıddıki, *Realistic modelling of quantum point contacts subject to high magnetic fields and with current bias at out of linear response regime,* arXiv: 0803.3543v1

[12] H. Van Houten, C. W. J. Beenakker, B. J. Van wees, *Quantum Point Contacts* (Academic Press, 1992)

[13] Douglas C. Giancoli, *Physics for Scientists & Engineers with Modern Physics* (3th ed.) (Prentice Hall, 2000)

[14] R. Resnick, D. Halliday, K. S. Krane, *Physics* (4th ed.) (John Wiley & Sons, 1992)

[15] N. W. Aschcroft, N. D. Mermin, *Solid state Physics* (Harcourt College Publishers, 1976)

[16] D. Yoshioka, *The Quantum Hall Effect* (Springer, 2002)

[17] Keshav N. Shrivastava, *Introduction to Quantum Hall Effect* (Nova Science Publishers, 2002)

[18] Afif Sıddıki, *Modeling Two-Dimensional Charge Devices*

[19] R. J. Haug, *Edge-state transport and its experimental consequences in high magnetic fields,* Semicond. Sci. Technol. 8 (1993) 131

[20] C. L. Kane, M. P. A. Fisher, *Edge state transport*

[21] www.tf.uni-kiel.de/matwis/amat/elmat_en/kap_1/backbone/r1_3_2.html

[22] http://www.warwick.ac.uk/~phsbm/qhe.htm